AFRL-RX-WP-JA-2015-0160

THE EFFECT OF FORGING VARIABLES ON THE SUPERSOLVUS HEAT-TREATMENT RESPONSE OF POWDER-METALLURGY NICKEL-BASE SUPERALLOYS (POSTPRINT)

S.L. Semiatin and A.L. Pilchak
Air Force Research Laboratory

J.M. Shank and A.R. Shiveley
UES, Inc.

W.M. Saurber and E.F. Gaussa
Materials & Manufacturing Directorate, AFRL

W.K. Lewis, K. A. S. Fernando, and E.A. Guliants
University of Dayton

OCTOBER 2014
Interim Report

AIR FORCE RESEARCH LABORATORY
MATERIALS AND MANUFACTURING DIRECTORATE
WRIGHT-PATTERSON AIR FORCE BASE OH 45433-7750
AIR FORCE MATERIEL COMMAND
UNITED STATES AIR FORCE

NOTICE AND SIGNATURE PAGE

Using Government drawings, specifications, or other data included in this document for any purpose other than Government procurement does not in any way obligate the U.S. Government. The fact that the Government formulated or supplied the drawings, specifications, or other data does not license the holder or any other person or corporation; or convey any rights or permission to manufacture, use, or sell any patented invention that may relate to them.

Qualified requestors may obtain copies of this report from the Defense Technical Information Center (DTIC) (http://www.dtic.mil).

AFRL-RX-WP-JA-2015-0160 HAS BEEN REVIEWED AND IS APPROVED FOR PUBLICATION IN ACCORDANCE WITH ASSIGNED DISTRIBUTION STATEMENT.

//Signature//

S.L. SEMIATIN, Project Engineer
Metals Branch
Structural Materials Division

//Signature//

DANIEL J. EVANS, Chief
Metals Branch
Structural Materials Division

//Signature//

ROBERT T. MARSHALL, Deputy Chief
Structural Materials Division
Materials And Manufacturing Directorate

This report is published in the interest of scientific and technical information exchange and its publication does not constitute the Government's approval or disapproval of its ideas or findings.

REPORT DOCUMENTATION PAGE

Form Approved
OMB No. 0704-0188

1. REPORT DATE *(DD-MM-YY)*	2. REPORT TYPE	3. DATES COVERED *(From - To)*
October 2014	Interim	19 March 2014 – 26 September 2014

4. TITLE AND SUBTITLE
THE EFFECT OF FORGING VARIABLES ON THE SUPERSOLVUS HEAT-TREATMENT RESPONSE OF POWDER-METALLURGY NICKEL-BASE SUPERALLOYS (POSTPRINT)

5a. CONTRACT NUMBER
In-house

5b. GRANT NUMBER

5c. PROGRAM ELEMENT NUMBER
62102F

6. AUTHOR(S)
See back.

5d. PROJECT NUMBER
4349

5e. TASK NUMBER

5f. WORK UNIT NUMBER
X0W6

7. PERFORMING ORGANIZATION NAME(S) AND ADDRESS(ES)
See back.

8. PERFORMING ORGANIZATION REPORT NUMBER

9. SPONSORING/MONITORING AGENCY NAME(S) AND ADDRESS(ES)
Air Force Research Laboratory
Materials and Manufacturing Directorate
Wright-Patterson Air Force Base, OH 45433-7750
Air Force Materiel Command
United States Air Force

10. SPONSORING/MONITORING AGENCY ACRONYM(S)
AFRL/RXCM

11. SPONSORING/MONITORING AGENCY REPORT NUMBER(S)
AFRL-RX-WP-JA-2015-0160

12. DISTRIBUTION/AVAILABILITY STATEMENT
Distribution Statement A. Approved for public release; distribution unlimited.

13. SUPPLEMENTARY NOTES
PA Case Number: 88ABW-2014-0747, Clearance Date: 26 February 2014. Journal article published in *Metallurgical and Materials Transactions A,* Volume 45A, December 2014—6231. © 2014 The Minerals, Metals & Materials Society and ASM International. The U.S. Government is joint author of the work and has the right to use, modify, reproduce, release, perform, display or disclose the work. This report contains color. The final publication is available at DOI: 10.1007/s11661-014-2572-y.

14. ABSTRACT

The effect of subsolvus forging temperature and strain rate on the grain size developed during final supersolvus heat treatment (SSHT) of two powder-metallurgy, gamma–gamma prime superalloys, IN-100 and LSHR, was established. For this purpose, isothermal, hot compression tests were performed at temperatures ranging from 1144 K (871°C) and 22 K (22°C) below the respective gamma-prime solvus temperatures (T*ý*) and strain rates between 0.0003 and 10 s^{-1}. Deformed samples were then heat treated 20 K (20°C) above the solvus for 1 h with selected additional samples exposed for shorter and longer times. For both alloys, the grain size developed during SSHT was in the range of 15 to 30 μm, except for those processing conditions consisting of pre-deformation at the highest temperature, i.e., T*ý*—22 K (T*ý*—22°C), and strain rates in the range of ~0.001 to 0.1 s^{-1}. In these latter instances, the heat-treated grain size was approx. four times as large. The observations were interpreted in terms of the mechanisms of deformation during hot working and their effect on the driving forces for grain-boundary migration which controls the evolution of the gamma-grain size.

15. SUBJECT TERMS
crystallographic gradient, metal, microstructural gradient

16. SECURITY CLASSIFICATION OF:			17. LIMITATION OF ABSTRACT:	18. NUMBER OF PAGES	19a. NAME OF RESPONSIBLE PERSON (Monitor)
a. REPORT	b. ABSTRACT	c. THIS PAGE			S.L. Semiatin
Unclassified	Unclassified	Unclassified	SAR	25	19b. TELEPHONE NUMBER *(Include Area Code)* (937) 255-1345

REPORT DOCUMENTATION PAGE Cont'd

6. AUTHOR(S)

S.L. Semiatin and A.L. Pilchak - Materials and Manufacturing Directorate, Air Force Research Laboratory

J.M. Shank and A.R. Shiveley - UES, Inc.

W.M. Saurber and E.F. Gaussa - University of Dayton

7. PERFORMING ORGANIZATION NAME(S) AND ADDRESS(ES)

Air Force Research Laboratory
Materials and Manufacturing Directorate
Wright-Patterson AFB, Ohio 45433

UES, Inc.
4401 Dayton-Xenia Road
Dayton, Ohio 45432

University of Dayton
300 College Park
Dayton, Ohio 45409

The Effect of Forging Variables on the Supersolvus Heat-Treatment Response of Powder-Metallurgy Nickel-Base Superalloys

S.L. SEMIATIN, J.M. SHANK, A.R. SHIVELEY, W.M. SAURBER, E.F. GAUSSA, and A.L. PILCHAK

The effect of subsolvus forging temperature and strain rate on the grain size developed during final supersolvus heat treatment (SSHT) of two powder-metallurgy, gamma–gamma prime superalloys, IN-100 and LSHR, was established. For this purpose, isothermal, hot compression tests were performed at temperatures ranging from 1144 K (871 °C) and 22 K (22 °C) below the respective gamma-prime solvus temperatures ($T_{\gamma'}$) and strain rates between 0.0003 and 10 s^{-1}. Deformed samples were then heat treated 20 K (20 °C) above the solvus for 1 h with selected additional samples exposed for shorter and longer times. For both alloys, the grain size developed during SSHT was in the range of 15 to 30 μm, except for those processing conditions consisting of pre-deformation at the highest temperature, *i.e.*, $T_{\gamma'}$—22 K ($T_{\gamma'}$—22 °C), and strain rates in the range of ~0.001 to 0.1 s^{-1}. In these latter instances, the heat-treated grain size was approx. four times as large. The observations were interpreted in terms of the mechanisms of deformation during hot working and their effect on the driving forces for grain-boundary migration which controls the evolution of the gamma-grain size.

DOI: 10.1007/s11661-014-2572-y

I. INTRODUCTION

NICKEL-BASE superalloys are widely used for high-temperature, rotating components in the aerospace-propulsion and land-based, power-generation industries.[1] The ability to obtain uniform composition and to control microstructure *via* powder-metallurgy (PM) techniques underlies the production and application of a large number of commercial superalloys. Typically synthesized *via* spray atomization, superalloy powders are consolidated by hot isostatic pressing, blind-die compaction, hot extrusion, or a combination of such methods to produce billet. Billet-processing parameters are selected to enable the development of a uniform, two-phase microstructure with fine gamma-grain and precipitate sizes of the order of several microns. Such a microstructure leads to superplastic behavior (low flow stress, high strain-rate sensitivity) during subsequent part fabrication *via* isothermal forging at temperatures below the solution temperature (solvus) of the structure-control precipitates.

S.L. SEMIATIN, Senior Scientist, Materials Processing/Processing Science, and A.L. PILCHAK, Research Leader, Metallic Materials and Processes, are with the Air Force Research Laboratory, Materials and Manufacturing Directorate, AFRL/RXCM, Wright Patterson Air Force Base, OH 45433. Contact e mail: sheldon.semiatin@us.af.mil J.M. SHANK, Technician, and A.R. SHIVELEY, Research Scientist, are with UES, Inc., 4401 Dayton Xenia Road, Dayton, OH 45432. W.M. SAURBER and E.F. GAUSSA, Undergraduate Students, are with the Department of Mechanical and Aerospace Engineering, University of Dayton, 300 College Park, Dayton, OH 45409.
Manuscript submitted March 7, 2014.
Article published online September 26, 2014

A number of investigations have been conducted to establish the interrelation between the microstructure of PM superalloys and the plastic-flow response at subsolvus temperatures and thus aid in the definition of the processing window for isothermal forging.[2–9] Many of these efforts have utilized superalloys with a microduplex structure of gamma grains and gamma-prime precipitates. Three distinct behaviors depending on the initial gamma grain size relative to the critical grain size characteristic of superplastic flow have been noted. When the initial grain size is less than, equal to, or greater than the critical value, flow-hardening, steady-state, or flow-softening behavior is observed, respectively. In turn, these three types of observations can be ascribed to dynamic grain growth, classical superplastic flow under nearly-constant grain-size conditions, and dynamic recrystallization to a finer grain size. Furthermore, grain-size coarsening or refinement has been shown to lead to transitions between so-called stage II (superplastic) flow largely characterized by grain/interphase boundary sliding and stage III (power-law-creep) flow primarily due to the glide and climb of dislocations within the interior of grains.

Other research on the thermomechanical processing (TMP) of PM superalloys has focused on the effect of isothermal-forging conditions on the evolution of gamma grain size during final supersolvus heat treatment (SSHT), which is often used to obtain a coarser, more creep-resistant microstructure. A number of these efforts have concerned those forging parameters that give rise to highly-undesirable abnormal grain growth (AGG). For instance, Soucail, Huron, and their coworkers[10,11] have shown that subsolvus isothermal

forging at strain rates near the transition from stage II to stage III plastic flow are quite detrimental with regard to AGG during subsequent SSHT. In addition, it has been suggested that variables such as subsolvus exposure temperature, the heating rate to the solvus (and thus the rate at which gamma-prime pinning particles dissolve), and the location of pinning particles relative to larger or smaller grains in the grain-size distribution may also play an important role in the occurrence of AGG.[12–15] Based on these fundamental investigations, the efficacy of processing routes that impose an upper limit on the strain rate during isothermal forging (to maintain superplastic conditions) and the control of carbon level (to ensure a minimum amount of various carbide phases which are stable above the solvus and can pin the gamma grain boundaries) on preventing AGG has been demonstrated.[16–19]

The use of a higher subsolvus forging temperature and lower strain rate relative to typical practices (*i.e.*, a so-called "hot/slow" approach) has been proposed as a method to prevent AGG but still obtain a relatively coarse, more-creep-crack-growth-resistant microstructure during SSHT.[20] Recent work[21] has confirmed such an approach for the PM superalloy LSHR. Specifically, forging at a temperature ~20 K (20 °C) below the solvus temperature at a rate between 0.0005 and 0.01 s^{-1} produced an average gamma grain size during SSHT approximately three times that obtained *via* typical forging practices. This result was interpreted in terms of the effect of forging variables on the location of the primary gamma-prime precipitates (at gamma grain boundaries vs grain interior locations) and the subsequent non-uniform dissolution of these precipitates and release of the associated pinning pressure during SSHT.

The present work was undertaken to provide further insight into the effect of standard and non-standard forging parameters on grain structure development during final SSHT. To this end, samples of two PM superalloys, IN-100 and LSHR, were subjected to isothermal hot compression testing over broad ranges of strain rate and temperature followed by SSHT. Backscatter-electron imaging and electron-backscatter diffraction were used to establish the effect of forging parameters on the details of gamma-grain and gamma-prime-precipitate evolution and thus provide a basis for interpreting those factors that may affect grain-structure evolution during SSHT.

II. MATERIALS AND PROCEDURES

A. *Materials*

Two different PM superalloys, IN-100 and LSHR, were used to determine the effect of isothermal forging parameters on as-forged and forged-and-SSHT microstructure evolution. PM IN-100, a proprietary alloy of Pratt and Whitney, is widely used for the manufacture of jet-engine disks. The PM superalloy LSHR (denoting "low-solvus, high refractory") was developed by NASA for jet-engine disks as well. Both alloys provide an attractive balance of properties at the bore and rim of disks that have been subjected to a graded-microstructure heat treatment in which only the component rim is exposed above the solvus temperature to promote local growth of the gamma grains.[22,23]

The IN-100 material was received from Pratt and Whitney as 89-mm-diameter bar that had been extracted from the center of a larger-diameter extruded billet. Its nominal composition is given in Table I. In the as-received condition, the microstructure consisted primarily of fine gamma grains and gamma-prime precipitates, each of whose average diameter was ~1.5 μm. There was also ~0.35 vol pct of carbide and boride particles whose average diameter was ~230 nm. These particles appeared as stringers whose spacing was not uniform but was generally in the range 20 to 40 μm. The gamma-prime solvus temperature, $T_{\gamma'}$, of this alloy was 1458 K (1185 °C).

The LSHR material consisted of 230-mm-diameter extruded billet produced by Special Metals (Princeton, KY). This was the same material as that used in two previous investigations of the TMP of LSHR.[21,24] Its composition is given in Table I; its processing history is summarized in detail in the previous papers. The microstructure of the as-received LSHR also comprised a fine, microduplex structure of gamma grains and gamma-prime precipitates, each of whose average diameter was ~2 μm, and ~0.33 vol pct of carbide/boride particles with an average diameter of 315 nm. In contrast to the carbides and borides in IN-100, those in the LSHR program material were more uniformly distributed in the matrix and did not form stringers. The gamma-prime solvus, $T_{\gamma'}$, of LSHR was 1430 K (1157 °C).

B. *TMP Approach*

Isothermal, hot compression testing and SSHT were used to evaluate plastic flow and microstructure evolution during thermomechanical processing (TMP) of the two PM superalloys For this purpose, cylindrical compression samples measuring 10-mm diameter × 15-mm height were electric-discharge machined from the two program materials.

Hot compression samples were first coated with glass for lubrication. Following lubrication, the sample and silicon–nitride compression tooling (which were mounted in a 250 kN servo-hydraulic test system) were induction heated using an iron-chromium-aluminum alloy susceptor to a test temperature which lay in the range between 1144 K (871 °C) and $T_{\gamma'}$—22 K ($T_{\gamma'}$—22 °C) in approximately 10 minutes. Following a soak at temperature for an additional 10 minutes, each sample was then compressed to an average axial (height) strain of 0.7.* Constant true strain rates lying between 0.0003 and 10 s^{-1} were used. Following compression, each sample was forced-air cooled.

*Compressive strains, strain rates, and stresses are reported as *positive* quantities here and throughout the balance of this work.

Table I. Chemical Composition (Weight Pct) of Program Materials

Material	Co	Cr	Al	Ti	Mo	W	Nb	Ta	V	C	B	Zr	Ni
IN 100*	18.5	12.4	5.0	4.3	3.2				0.8	0.07	0.02	0.06	bal.
Billet	20.4	12.3	3.5	3.5	2.7	4.3	1.5	1.5		0.045	0.027	0.05	bal.

*Composition for IN 100 is nominal; exact composition was proprietary.

True stress-true strain curves were determined from average pressure (p_{av})—axial strain (ε) plots derived from the compression load-stroke data which were reduced assuming uniform deformation and corrected for the test-machine compliance. The neglect of friction was estimated to lead to maximum errors in the flow stress of the order of 3 pct for the sample geometry and height reduction used in the present work.[30] Sample calculations of the effect of deformation heating on the flow response at strain rates of 0.1 s^{-1} or greater indicated that the qualitative flow hardening/softening response was unchanged by such corrections.

The strain-rate sensitivity of the flow stress (m value) was determined from the continuous flow curves at a strain of approximately 0.02 (*i.e.*, a strain at which variations in microstructure with strain rate were small) and strain-rate jump tests. The latter experiments were performed at various temperatures to an axial height strain of 1.1 to evaluate the evolution of the strain-rate sensitivity with strain. Most of these tests comprised imposing alternating strain rates, which differed by a factor of two within the range between 0.0005 and 0.01 s^{-1}, at strain increments of ~0.1. The uncertainty in the m values reported herein was estimated to be ±0.02.

To determine the effect of SSHT on microstructure evolution, sections of the deformed samples were encapsulated in quartz tubes backfilled with argon and furnace heat treated for 1 h at 1477 K (1204 °C) (IN-100) or 1444 K (1171 °C) (LSHR), followed by air cooling. Several sections were also given a SSHT for shorter or longer times to obtain a broad insight into grain-growth kinetics above the solvus. Last, several samples deformed at $T_{\gamma'}$—22 K ($T_{\gamma'}$—22 °C) were given a 1 hour heat treatment at this temperature prior to SSHT to assess the possible influence of subsolvus annealing on subsequent supersolvus microstructure response.

C. *Microstructure Characterization*

Following compression or compression + heat treatment, samples were sectioned axially. The sections were prepared using standard metallographic techniques, finishing by polishing with 0.05-μm colloidal silica.

Microstructures were characterized using backscattered-electron (BSE) imaging and electron backscatter diffraction (EBSD) in scanning electron microscopes (SEMs) equipped with field-emission guns (Sirion for BSE and XL-30 for EBSD, both manufactured by FEI, Hillsboro, OR) and EDAX/TSL OIM™ software (EDAX Corp., Mahwah, NJ). EBSD scans were performed over areas consisting of at least ~1000 grains using a step size between 0.2 and 5 μm; the specific parameters depended on the coarseness of the microstructure.

The average grain size, "as-large-as" (ALA) grain size, and grain-size distribution (GSD) for each material and set of processing conditions were determined using the grain-delineation software in the EDAX/TSL OIM™ system. During such evaluations, twins were removed automatically by applying the twin-removal ($\Sigma3$, $\Sigma9$ boundary) capability in the OIM™ software. Per the work of Wright,[25] grains were defined for most of the samples using a minimum boundary misorientation of 5 deg and a minimum size of 10 pixels. The size of each individual grain was then taken as the diameter (D) of a circle with area equivalent to that observed in section, and was thus an underestimate of the true (three-dimensional) diameter.

For samples compressed at subsolvus temperatures, the primary gamma-prime particles possessed orientations that were different from those of the adjacent gamma grains and exhibited similar Z-contrast. Hence, the reported grain sizes for most of these samples are averages of both the gamma and gamma-prime phases. For selected as-subsolvus-compressed samples, however, the two microstructural features were segmented using one of two different methods. The first, or simpler, technique comprised the application of an EBSD cleanup criterion to separate the microstructural features for samples compressed 22 K (22 °C) below the solvus at which temperature the sizes of the gamma-prime precipitates and gamma grains were greatly different. In essence, this approach comprised the elimination of grains whose number of pixels (typically ~25 pixels for a step size of 0.5 μm and ~50 pixels for a step size of 0.3 μm) just exceeded the area of the largest gamma-prime particles noted in BSE images. Examination of resulting grain-ID-map data revealed that approximately one-half to two-thirds of the "grains" were thus eliminated, or a number comparable to the BSE-image-determined ratio of the number of gamma prime particles to the number of gamma grains + gamma prime particles. Nevertheless, it should be emphasized that some of the gamma grains which had been sectioned far from their centroids may have also been eliminated by this method as well. Hence, the cleanup-criterion method of segmentation tended to produce an *upper* bound for the gamma grain size.

The second, more precise, "EBSD/EDS" segmentation method was quite time-consuming and thus applied to only several samples. This approach was based on the different chemical composition of the two major phases as inferred from SEM scans in which both EBSD and energy-dispersive-spectroscopy (EDS) composition data were collected.[26]

The average size and location of the primary gamma-prime precipitates relative to the gamma grain boundaries were also determined for samples deformed at 22 K (22 °C) below the solvus *via* hand painting and analysis of BSE micrographs using FoveaPro™ (Reindeer Graphics, Asheville, NC) and Adobe Photoshop® software.

For samples that were supersolvus heat treated following hot compression, the gamma-prime precipitates were very fine because of the moderately rapid final cooling rate. There was no effect of these precipitates on grain-size analysis because of their coherence with the gamma-grain matrix.

III. RESULTS

The principal results from this research consisted of the plastic-flow response in terms of stress–strain curves and values of the strain-rate sensitivity and characterization of the as-deformed and deformed-and-SSHT microstructures *via* BSE imaging and EBSD.

A. *Plastic-Flow Response*

1. *Flow curves*

True stress-true strain curves exhibited a range of shapes depending on test temperature and strain rate (Figures 1 and 2). For IN-100, the flow response at the lowest test temperature [1144 K (871 °C)] and all strain rates consisted of an initial strain-hardening stage which was followed by a peak stress, flow softening, and then near-steady-state flow at large strains (Figure 1(a)); these features are indicative of discontinuous dynamic recrystallization (DDRX). At the intermediate hot-working temperature of 1255 K (982 °C) (Figure 1(b)), the flow stresses were lower, but all of the flow curves were also typical of DDRX, except the observation for the lowest strain rate (0.0003 s^{-1}) for which flow-softening was minimal. This latter behavior is suggestive of near-superplastic deformation.

For deformation at 1339 K (1066 °C), a temperature within the range often used for isothermal forging of PM superalloys, the IN-100 flow curves exhibited near-steady-state or steady-state flow (typical of superplasticity) at the lowest strain rates and flow-softening (suggestive of DDRX) at high strain rates (Figure 1(c), (d)). The transition between the two regimes occurred at a strain rate of approximately 0.001 s^{-1}. A similar transition between a DDRX-type flow response and superplastic/steady-state flow was also found at the highest subsolvus test temperature [1436 K (1163 °C)], which was 22 K (22 °C) below the gamma-prime solvus (Figure 1(e)). At this temperature, the transition occurred at a strain rate between approximately 0.01 and 0.003 s^{-1}. At strain rates below ~0.003 s^{-1}, the nature of the flow response changed yet again from steady-state flow to flow hardening (Figure 1(f)), the latter behavior typically ascribed to dynamic grain growth.[21]

Except for slightly higher flow stresses, the flow response for the LSHR in terms of its dependence on temperature and strain rate was similar to the observations for IN-100. A few measurements are shown in Figure 2; more detailed discussion of the flow behavior of LSHR can be found in Reference 21. In brief, the transition from DDRX to superplastic behavior appeared to occur at a strain rate of ~0.01 s^{-1} at both 1339 K and 1408 K (1066 °C and 1135 °C), the latter temperature lying 22 K (22 °C) below the solvus. The stress–strain curves for deformation just below the solvus also indicated flow hardening at a strain rate of 0.0005 s^{-1}.

2. *Strain-rate-sensitivity data*

Somewhat more quantitative insight into plastic-flow behavior and pertinent deformation mechanisms was obtained from measurements of the strain rate sensitivity of the flow stress (m values) determined from continuous flow curves at a true strain of 0.02 (Figure 3) and strain-rate jump tests over large ranges of strain (Tables II, III, and IV).

For IN-100, the continuous flow curves revealed relatively low m values (≤0.3) at 1144 K (871 °C) over the entire strain rate range (Table II); these m's are typical of deformation controlled by intragranular dislocation glide/climb processes that can give rise to DDRX at hot-working temperatures. For the next highest temperature, 1255 K (982 °C), the m values were slightly higher (≤0.4), except for the lowest strain rate (~0.0002 s^{-1}) at which m was equal to 0.6. These observations indicate a transition from dislocation glide/climb processes at the higher strain rates to superplastic flow (characterized by $m \geq 0.5$) at the lowest strain rate. Similar transitions from high m (superplastic) to low m (dislocation glide/climb) behavior were also seen in the rate sensitivity results from the continuous flow curves at 1339 K and 1436 K (1066 °C and 1163 °C) (Table II). At these temperatures, the transition strain rates were approximately 0.01 and 0.003 s^{-1}, respectively. These transition strain rates were slightly higher or comparable to those deduced from the shape of the flow curves at the respective temperatures.

The small differences between the transition strain rate deduced from the shape of the flow curves and the low-strain m-values were partially clarified by analysis of the dependence of the rate sensitivity on strain, as determined from the strain-rate-jump tests (Table III). The data for 1339 K (1066 °C) showed a relatively constant m value (*i.e.*, 0.64 to 0.68) over the entire strain range between 0.1 and 0.85 for the jump test involving the strain-rate range of 0.001 to 0.002 s^{-1}. In light of the continuous-flow-curve results, the transition strain rate at this temperature for large strains is thus likely between 0.002 and 0.01 s^{-1}.

The plastic-flow behavior exhibited by the IN-100 jump tests at 1436 K (1163 °C) was somewhat more complex. The results for the ranges of 0.0002 to 0.0004 s^{-1} and 0.001 to 0.002 s^{-1} both showed a superplastic value of m at low strains, but a decrease in m to values less than 0.5 with increasing strain. These strain rate regimes are also those for which flow-hardening response, indicative of dynamic grain growth, was noted in the stress–strain curves (Figure 1(f)). Thus, it may be deduced that superplastic behavior was lost

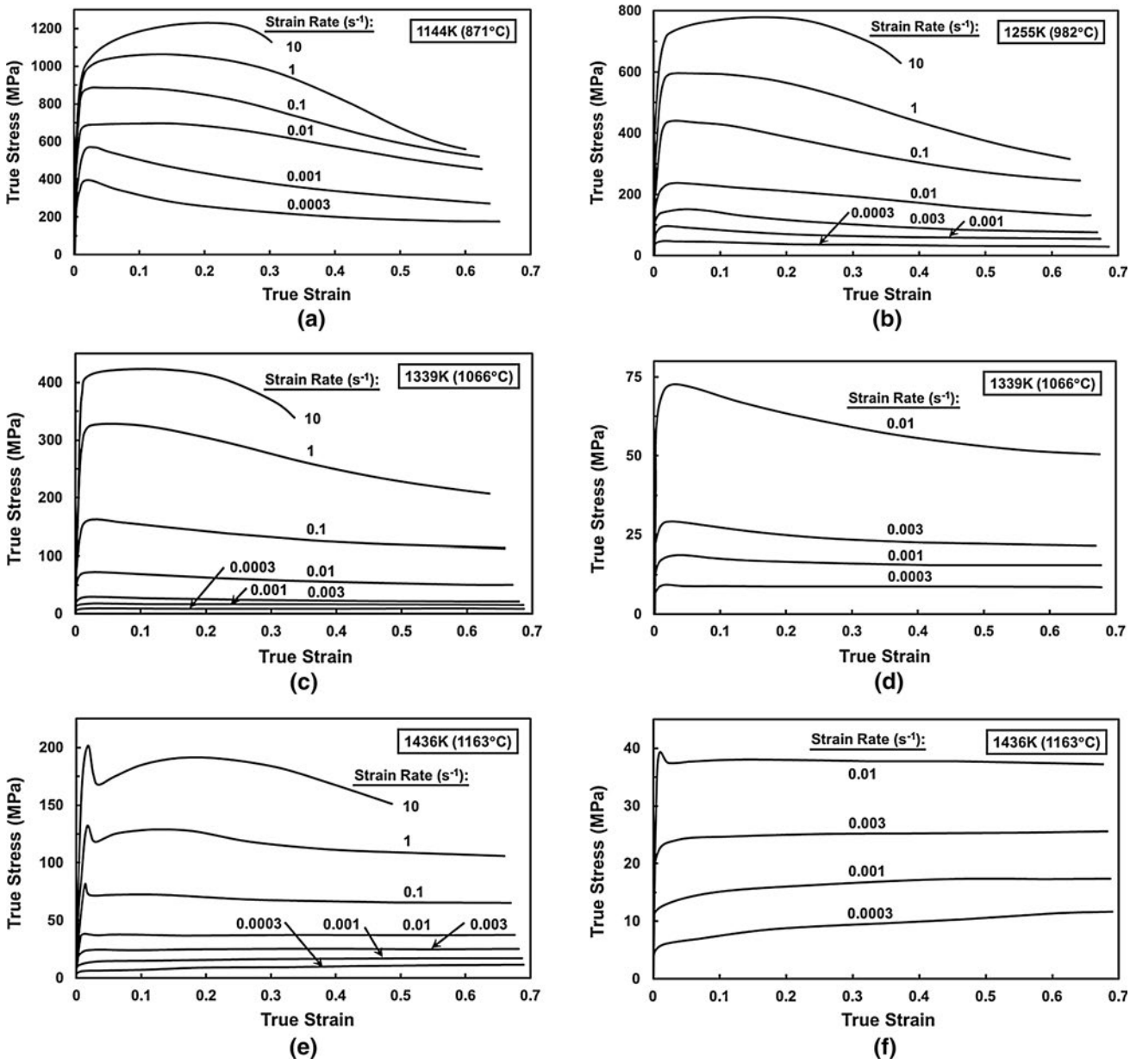

Fig. 1 Constant strain rate flow curves for IN 100 determined at test temperatures of (*a*) 1144 K (871 °C), (*b*) 1255 K (982 °C), (*c*, *d*) 1339 K (1066 °C), or (*e*, *f*) 1436 K (1163 °C).

with increasing strain due to grain growth. For the strain-rate ranges of 0.003 to 0.006 s^{-1} and 0.01 to 0.02 s^{-1}, the m values at 1436 K (1163 °C) were all in the range of 0.2 to 0.35 over the entire range of imposed strain and thus suggested that deformation was controlled by dislocation glide/climb and comprised a major component of DDRX.

The strain-rate sensitivity for LSHR showed similar trends. At the typical temperature for isothermal forging, 1339 K (1066 °C), and that lying 22 K (22 °C) below the gamma-prime solvus, m values from the continuous flow curves were typical of superplasticity at strain rates below 0.01 s^{-1} and DDRX for strain rates of 0.01 s^{-1} or greater (Table IV). Similar to the observations for IN-100, jump-test results over the strain-rate range of 0.0005 to 0.001, which were reported in prior work,[21] showed a retention of superplastic values of m at 1339 K (1066 °C) to large strains, but a gradual loss with increasing strain of such characteristics at $T_{\gamma'}$—22 K ($T_{\gamma'}$—22 °C).

B. *Microstructure Characterization*

1. *As-deformed condition*

Observations from BSE images and EBSD average grain/precipitate-size measurements for IN-100 verified and expanded upon hypotheses regarding microstructure evolution during deformation deduced from the plastic-flow response described in Section III.A. For test temperatures of 1144 K and 1255 K (871 °C and

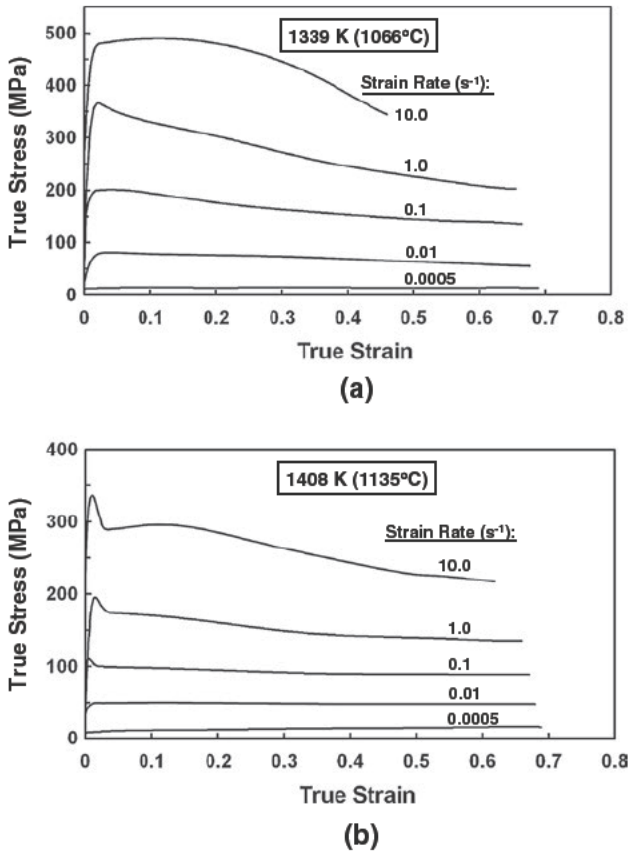

Fig. 2 Constant strain rate flow curves for LSHR determined at test temperatures of (*a*) 1339 K (1066 °C) or (*b*) 1408 K (1135 °C).

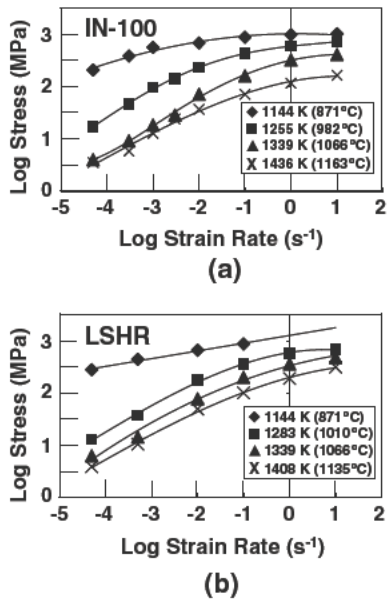

Fig. 3 Log stress *vs* log strain rate plots for (*a*) IN 100 and (*b*) LSHR. The stress corresponds to a true strain of 0.02.

982 °C), for example, comparison of the as-preheated microstructures to those developed during deformation revealed grain refinement as a result of DDRX (Table V; Figure 4).

For samples deformed at 1339 K (1066 °C), the average sizes (and size distributions) of the gamma grains and the gamma-prime precipitates (as determined by the EBSD/EDS analysis to segment the two phases) were similar. However, the EBSD-determined average grain/precipitate size did show a measurable dependence on strain rate (Table V; Figure 5). At the two lower strain rates (0.0003 and 0.001 s^{-1}), the grain size after deformation was comparable to or slightly coarser than the as-preheated one, thus supporting the earlier conclusions regarding superplastic flow with perhaps a small amount of dynamic grain growth. At strain rates of 0.01 s^{-1} and greater, grain refinement whose degree increased with increasing strain rate was observed, most likely as a result of DDRX. Little change in grain size was noted for the intermediate strain rate, 0.003 s^{-1}. Based on the grain size trend for the higher strain rates, the appearance of retained work in the microstructure (Figure 6(c)), and flow softening for the corresponding stress–strain curve (Figure 1(d)), it appears that an element of DDRX had thus also occurred at 0.003 s^{-1}.

The EBSD-determined average grain/precipitate size developed during deformation 22 K (22 °C) below the gamma-prime solvus temperature (*i.e.*, 1436 K, or 1163 °C) showed a more complex behavior (Table V; Figure 6) than that observed at the lower test temperatures. At this temperature, the average gamma-prime-precipitate size, *i.e.*, ~1.5 to 2 μm, was considerably smaller than the average gamma-grain size in the as-deformed conditions (Tables V and VI) as well as after preheating alone. Hence, the EBSD values for the *average* gamma/gamma-prime size for these conditions (Table V) were *underestimates* of the actual gamma grain size. Based on the cleanup-criterion and EBSD/EDS methods, the gamma grain sizes (in μm) were estimated as 6.7 in the as-preheated condition and, following deformation at the various strain rates, to be approximately 8.7 (0.0003 s^{-1}), 8.3 (0.001 s^{-1}), 6.4 (0.003 s^{-1}), 6.9 (0.01 s^{-1}), 11 (0.1 s^{-1}), 12.8 (1 s^{-1}), and 8.1 μm (10 s^{-1}). Grain-*coarsening* thus appears to have occurred for the two lowest strain rates (0.0003 and 0.001 s^{-1}); this coarsening was as expected based on the flow hardening observed in the corresponding stress–strain data (Figure 1(f)). The small change in gamma-grain size at the two intermediate strain rates (0.003 and 0.01 s^{-1}) mirrored the borderline superplastic/DDRX trend postulated based on the plastic-flow response.

For the three highest strain rates at 1436 K (1163 °C), DDRX was evident from the flow curves (Figure 1(e)). The observed *increase* in grain size (Figures 6(e) and (f)) may be hypothesized to have resulted from the high flow stresses and thus high driving forces for boundary migration, an effect discussed further in Section IV. Furthermore, segmentation of the microstructures resulted in substantially lower values of the ALA:average grain-size ratios for the two highest strain rates in comparison to the un-segmented results, *i.e.*, ~3.3 and ~6.5. These latter values are comparable to those for the lower-temperature test conditions listed in Table V for which segmentation was not necessary because of the similarity in the sizes of the two microstructural constituents. In addition, these ratios were similar to or

Table II. Strain-Rate-Sensitivity Results from IN-100 Continuous Flow Curves ($\varepsilon = 0.02$)

Strain Rate Range (s^{-1})	1144 K (871 °C)	1255 K (982 °C)	1339 K (1066 °C)	1436 K (1163 °C)
0.0003 to 0.001	0.315	0.60	0.575	0.645
0.001 to 0.003		0.36	0.50	0.58
0.003 to 0.01		0.40	0.465	0.35
0.01 to 0.1	0.11	0.275	0.35	0.285
0.1 to 1	0.045	0.13	0.305	0.215

Table III. Strain-Rate-Sensitivity Results from IN-100 Jump Tests

Temp [K (°C)]	Strain Rate Range (s^{-1})	m ($\varepsilon \sim 0.1$)	m ($\varepsilon \sim 0.2$)	m ($\varepsilon \sim 0.85$)
1255 (982)	0.001 to 0.002	0.465	0.595	0.57
1339 (1066)	0.001 to 0.002	0.685	0.64	0.645
1436 (1163)	0.0002 to 0.0004	0.540	0.405	0.225
1436 (1163)	0.001 to 0.002	0.70	0.555	0.44
1436 (1163)	0.003 to 0.006	0.325	0.29	0.225
1436 (1163)	0.01 to 0.02	0.27	0.26	0.215

Table IV. Strain-Rate-Sensitivity Results from LSHR Continuous Flow Curves ($\varepsilon = 0.02$)

Strain Rate Range (s^{-1})	1339 K (1066 °C)	1436 K (1163 °C)
0.0005 to 0.01	0.565	0.515
0.01 to 0.1	0.41	0.315
0.1 to 1	0.255	0.275
1 to 10	0.12	0.22

Table V. EBSD Grain-Size Data for IN-100 Samples

Temp [K (°C)]/ Strain Rate (s^{-1})	As Preheated Avg/ ALA GS (μm)	As Compressed Avg/ ALA GS (μm)	Compressed + SSHT Avg/ALA GS (μm)
(As Rec'd)	(~1.5)		(20.5/91.8)
1144 (871)/0.001	~1.5	0.97/5.23	24.4/74.2
1255 (982)/0.001	1.79/7.55	1.50/5.16	24.9/69.5
1339 (1066)/0.0003	1.80/7.11	2.09/7.94	28.6/106.1
1339 (1066)/0.001	1.80/7.11	1.87/7.91	26.3/77.9
1339 (1066)/0.003	1.80/7.11	1.90/8.37	23.6/87.9
1339 (1066)/0.01	1.80/7.11	1.65/6.92	21.8/84.2
1339 (1066)/0.1	1.80/7.11	1.35/7.17	23.4/93.1
1339 (1066)/1	1.80/7.11	1.09/5.30	23.3/87.9
1436 (1163)/0.0003	4.93/20.8	6.97/29.9	35.6/224.0
1436 (1163)/0.001	4.93/20.8	6.32/23.8	79.0/399.9
1436 (1163)/0.003	4.93/20.8	4.8/23.5	90.3/309.6
1436 (1163)/0.01	4.93/20.8	4.85/31.8	86.8/305.8
1436 (1163)/0.1	4.93/20.8	5.36/36.4	41.6/137.6
1436 (1163)/1	4.93/20.8	5.19/83.1	21.8/72.7
1436 (1163)/10	4.93/20.8	3.99/27.2	21.3/73.3
1436 (1163)*	4.93/20.8		22.8/76.7

Grain tolerance angle 5 deg, cleanup 10 pixels, SSHT 1477 K (1204 °C)/1 h.
*Preheated at 1436 K (1163 °C) prior to SSHT.

slightly higher than those reported previously for annealed PM superalloys.[24]

Additional examination of BSE images, segmented EBSD/EDS data, and EBSD grain ID maps provided insight into the effect of test temperature on the location of the gamma-prime precipitates relative to the gamma grain boundaries (Table VI) and gamma-grain topology. As discussed below, the location of the primary gamma-prime precipitates appeared to be important with regard to the uniformity of their dissolution and concomitant migration of gamma grain boundaries during SSHT. Specifically, for deformation temperatures of 1339 K (1066 °C) and below, almost all of the gamma-prime precipitates were located at the gamma grain boundaries; that is to say, very few precipitates (<5 pct) were located totally within the gamma grains.

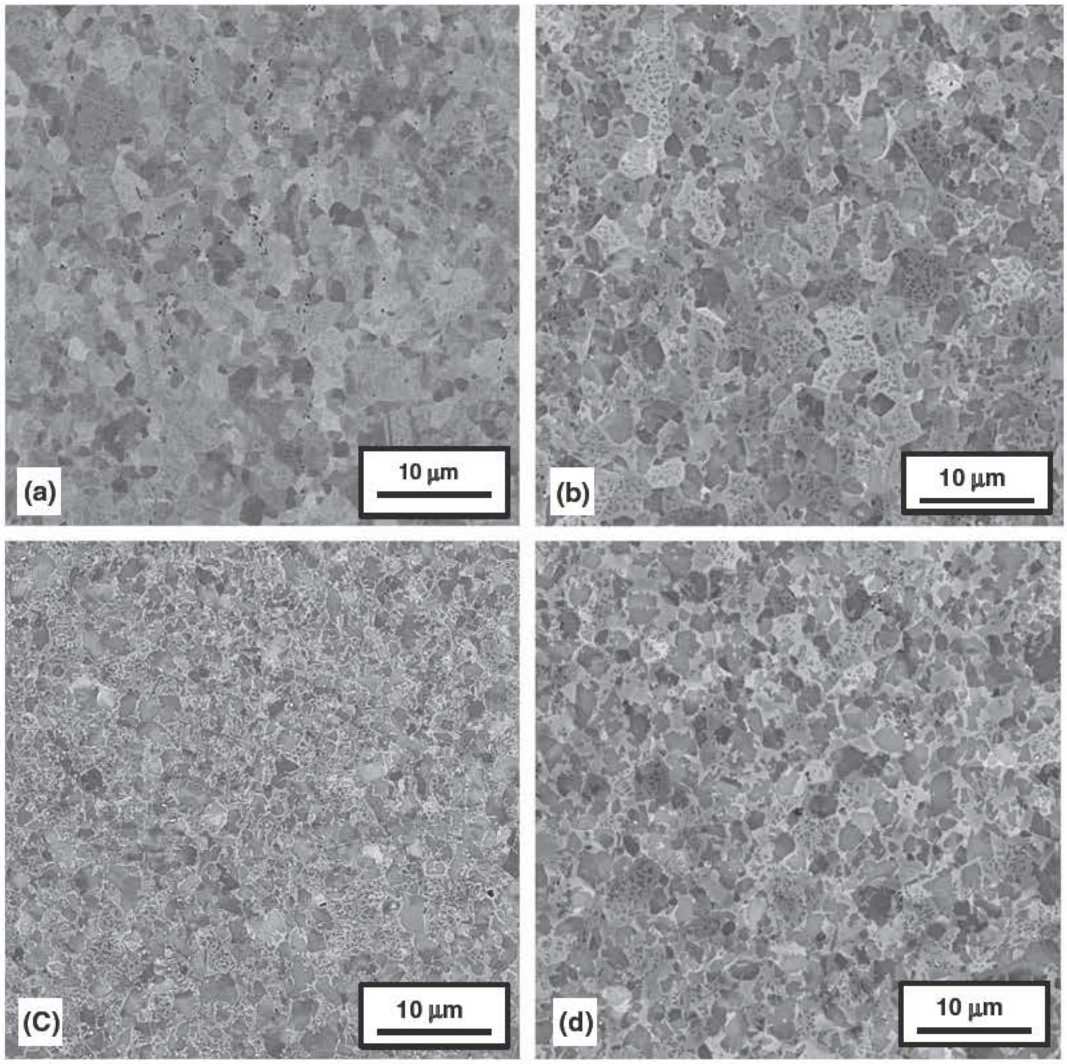

Fig. 4 BSE images illustrating the microstructure developed in IN 100 during preheating at (*a*) 1144 K (871 °C) or (*b*) 1255 K (982 °C) and *via* preheating and compression using a strain rate of 0.001 s^{-1} at (*c*) 1144 K (871 °C) or (*d*) 1255 K (982 °C).

By contrast, a modest-to-large fraction of gamma-prime particles was located *within* the gamma grains for samples deformed at 1436 K (1163 °C), *i.e.*, 22 K (22 °C) below the solvus temperature. Specifically, for a strain rate of 0.0003 s^{-1} (as well as material that was preheated but not deformed at this temperature), the fraction was ~30 pct. For strain rates in the range of 0.001 to 0.01 s^{-1}, the fraction was lower, ~10 to 25 pct. By contrast, at strain rates of 0.1 and 1 s^{-1}, the fraction increased substantially to ~50 or 70 pct, respectively. These high fractions are likely attributable to the higher flow stresses and dislocation densities at these strain rates, which in turn provide a large enough driving force to overcome gamma-prime pinning and thus enable gamma-grain-boundary migration. These observations are interpreted further in Section IV.

ALA grain sizes and gamma-grain-size histograms based on the EBSD data for IN-100 also revealed important differences between the microstructures of samples deformed at 1339 K (1066 °C) and those tested at 1436 K (1163 °C). For the former samples, the ALA grain sizes were all less than 10 μm (Table V; Figure 7(a)). For the samples deformed 22 K (22 °C) below the solvus temperature, the ALA (gamma) grain sizes were noticeably larger, *i.e.*, of the order of 23 to 30 μm for strain rates of 0.0003 to 0.01 s^{-1} and >30 μm for strain rates of 0.1 and 1 s^{-1} (Table V; Figure 7(b)). As will be shown in Section III–B–2, these sizes are respectively comparable to or greater than the apparent Zener limiting grain size of ~25 μm developed during SSHT.

Inspection of the EBSD grain ID maps for IN-100 samples deformed 22 K (22 °C) below the solvus temperature (*e.g.*, Figure 8) also revealed that relatively-equiaxed grain shapes were developed during plastic flow at strain rates of ~0.1 s^{-1} and greater, but that a small number of irregularly-shaped grains (indicated by arrows in Figures 8(a), (b)) were produced at the lower strain rates.

Microstructure evolution results for as-deformed LSHR were similar to those for IN-100 (Table VII). At temperatures of 1339 K (1066 °C) and below, the average grain sizes (1 to 2.5 μm) were similar to that of the as-received material (~2 μm) and can be attributed to DDRX and/or limited dynamic grain growth. During

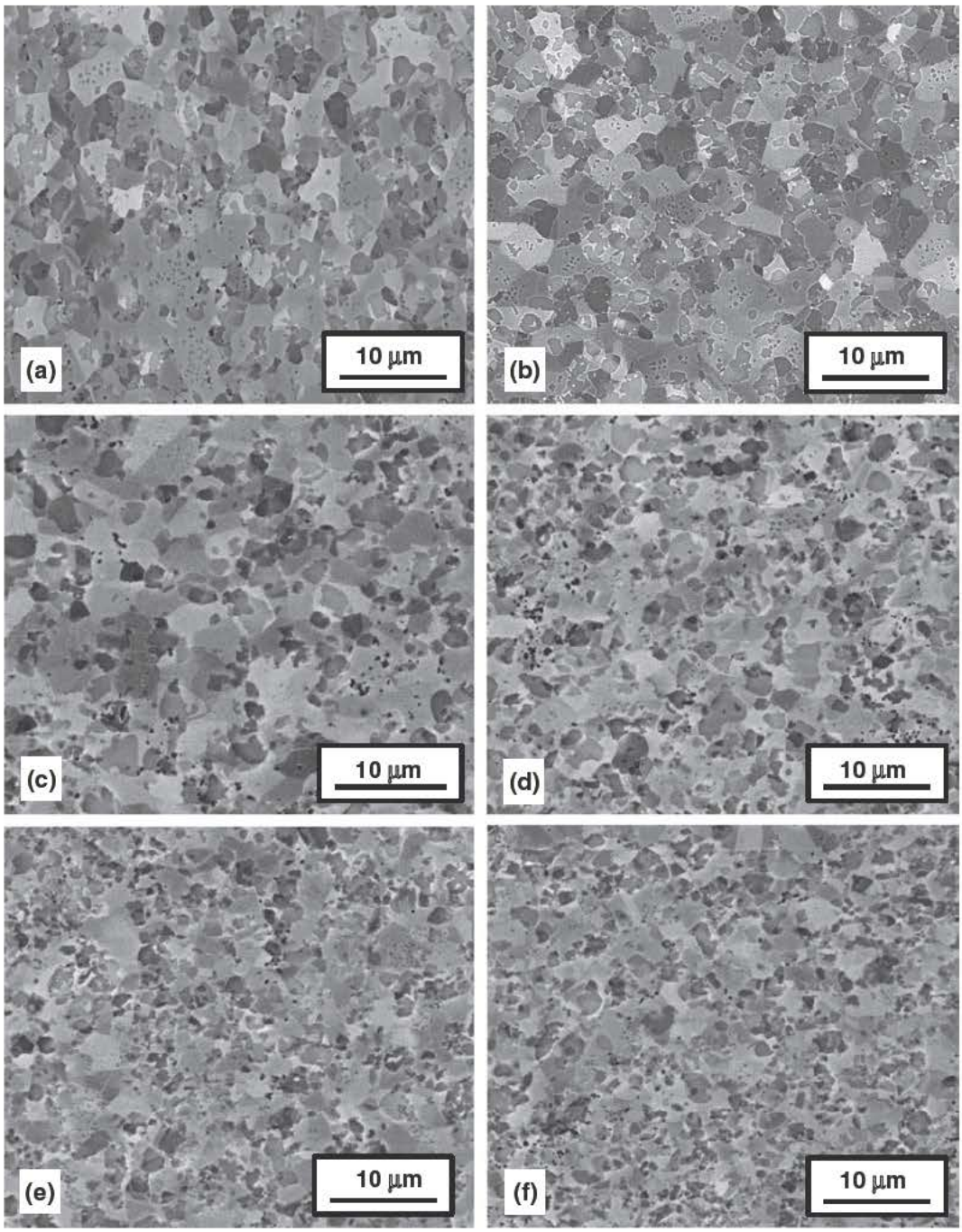

Fig. 5 BSE images illustrating the microstructures developed in IN 100 at 1339 K (1066 °C) (*a*) during preheating or during preheating and compression to a 2:1 height reduction at a strain rate (s^{-1}) of (*b*) 0.001, (*c*) 0.003, (*d*) 0.01, (*e*) 0.1, or (*f*) 1.

testing at 22 K (22 °C) below the solvus temperature (*i.e.*, 1408 K, or 1135 °C), deformation gave rise to microstructure coarsening due to dynamic grain growth (low strain rates) or DDRX and the migration of grain boundaries past gamma-prime precipitates (high strain rates).

2. *Deformed-and-SSHT condition*

The grain sizes developed in IN-100 during subsequent SSHT showed a marked dependence on previous hot-working conditions. All of the samples deformed at 1339 K (1066 °C) and below developed equiaxed gamma grain sizes in the range of 20 to 30 μm (Table V, Figures 9 and 10); this was also true of an as-received billet sample given the same SSHT. In addition, the ALA:average grain size ratios were all ~3 to 4 for these deformation conditions, similar to previous observations for SSHT samples of LSHR billet and pancake forgings.[24]

Microstructure evolution during SSHT of IN-100 samples pre-deformed 22 K (22 °C) below the solvus temperature (*i.e.*, 1436 K, or 1163 °C) contrasted

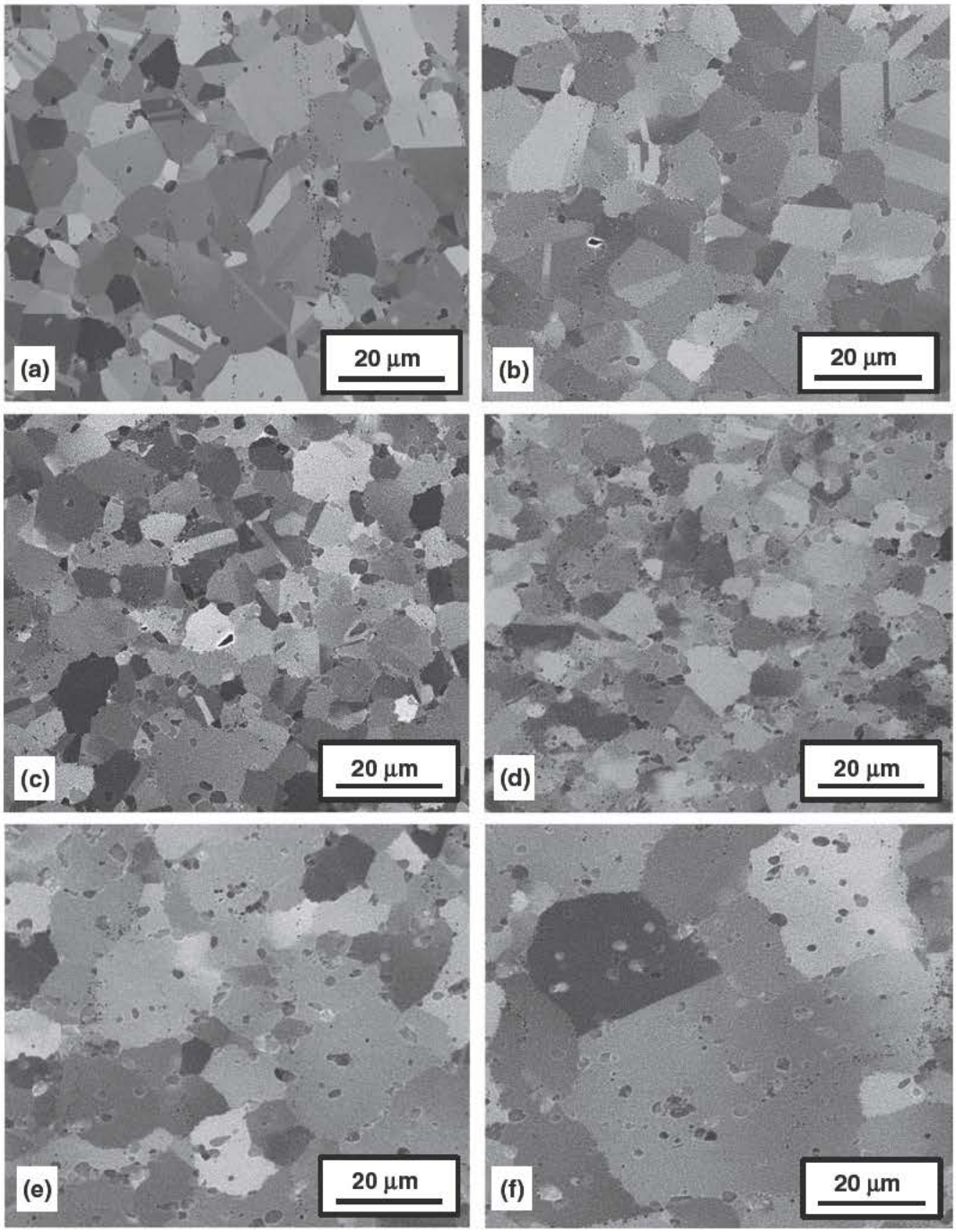

Fig. 6 BSE images illustrating the microstructures developed in IN 100 at 1436 K (1163 °C) (*a*) during preheating or during preheating and compression to a 2:1 height reduction at a strain rate (s^{-1}) of (*b*) 0.001, (*c*) 0.003, (*d*) 0.01, (*e*) 0.1, or (*f*) 1.

sharply with the observations for the other test conditions. Specifically, the average gamma grain size following SSHT for 1 hour exhibited low values (20 to 40 μm) for the lowest (0.0003 s^{-1}) and highest (1, 10 s^{-1}) imposed strain rates (as well as for a sample exposed but not deformed at this temperature) and higher values (~80 to 90 μm) for the intermediate strain rates (0.001 to 0.1 s^{-1}) (Table V). Examination of BSE images (Figures 11 and 12), EBSD grain ID maps (not shown), and the ALA results suggested however, that the observations were better binned into three groups corresponding to near-solvus deformation at very low, intermediate, or very high strain rates.

At the lowest strain rate (0.0003 s^{-1}), an apparently bimodal microstructure with both fine and coarse gamma grains was developed during the SSHT for 1 h. Although the average grain size was relatively small (35.6 μm), the ALA size was very large (224 μm) (Table V; Figure 11(a)). SSHT for different times of material deformed at this lowest rate (Table VIII) further indicated an unusual behavior suggesting periods of slower and faster increase of the average grain

size. Moreover, BSE micrographs for these various heat-treatment times (Figures 12(a), (c) and (e)) and measurements of the ALA grain size (Table VIII) showed a variety of unusual, non-equiaxed grain shapes and apparently erratic changes in the ALA grain size. Such observations were suggestive of an abnormal-like behavior (in which a relatively small fraction of "rogue" grains grow rapidly at the expense of surrounding grains) that had not become catastrophic.

The grain structures developed during SSHT of IN-100 deformed at the intermediate strain rates of 0.001, 0.003, and 0.01 s^{-1} were similar to each other. In each case, a variety of equiaxed and non-equiaxed shapes were observed for the 1 h heat treatments

Table VI. Gamma-Prime-Precipitate Data for As-Compressed IN-100 Samples

Temp [K (°C)]/Strain Rate (s^{-1})	Avg γ' Dia (μm) EDS/EBSD	Avg γ' Dia (μm) FoveaPro™	Pct Interior γ' EBSD/EDS	Pct Interior γ' FoveaPro™
1255 (982)/0.001	2.6		<1	
1339 (1066)/0.0003	2.7		3.8	
1339 (1066)/0.001	2.6		2.5	
1436 (1163)/ *		1.3		29.3
1436 (1163)/0.0003	2.6	1.5	25.8	29.1
1436 (1163)/0.001	2.4	1.6	15.6	18.1
1436 (1163)/0.003	3.1	1.4	9.2	19.3
1436 (1163)/0.01		1.8		23.9
1436 (1163)/0.1		1.8		48.7
1436 (1163)/1		1.8		69.3

*As preheated sample.

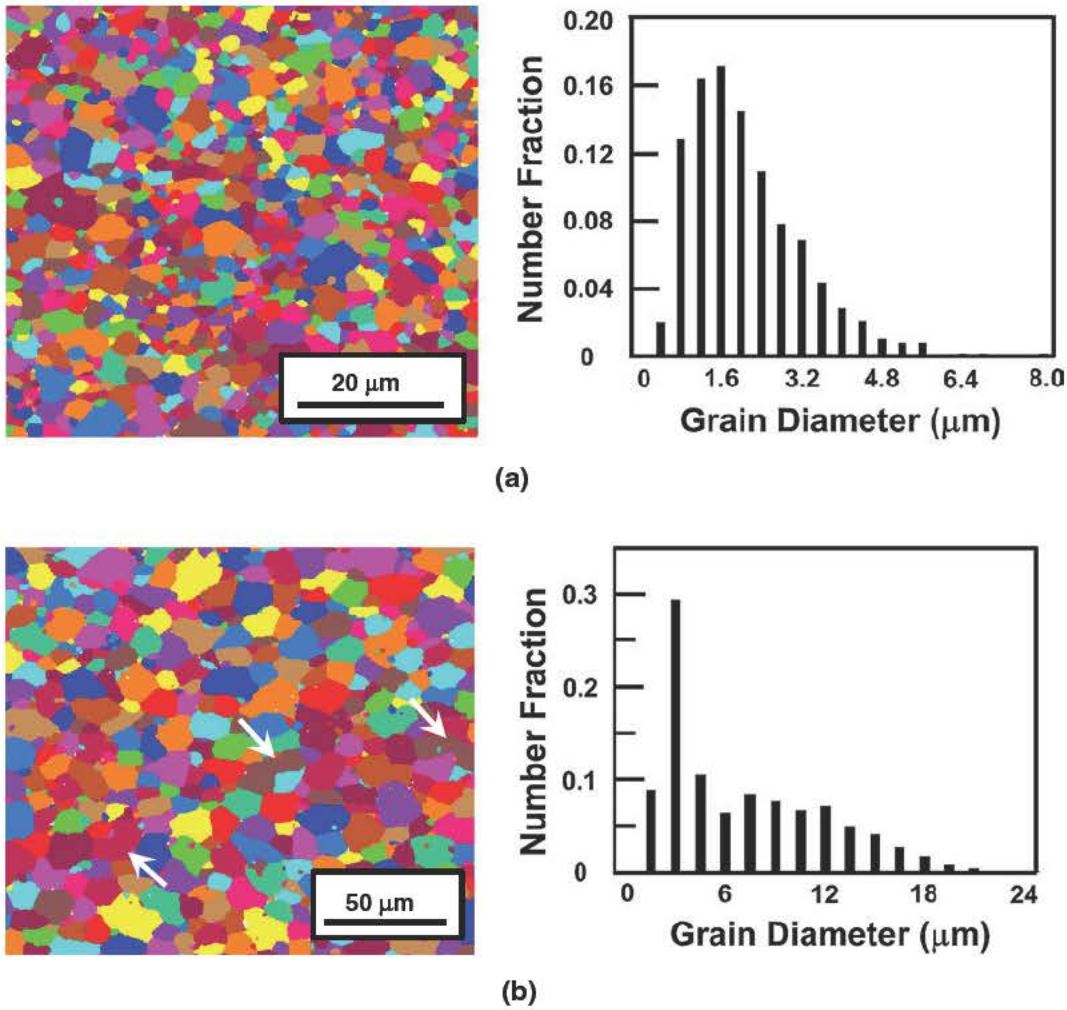

Fig. 7 Grain ID maps and grain size histograms derived from unsegmented EBSD data for IN 100 samples compressed to a 2:1 height reduction at a strain rate of 0.001 s^{-1} and a test temperature of (*a*) 1339 K (1066 °C) or (*b*) 1436 K (1163 °C).

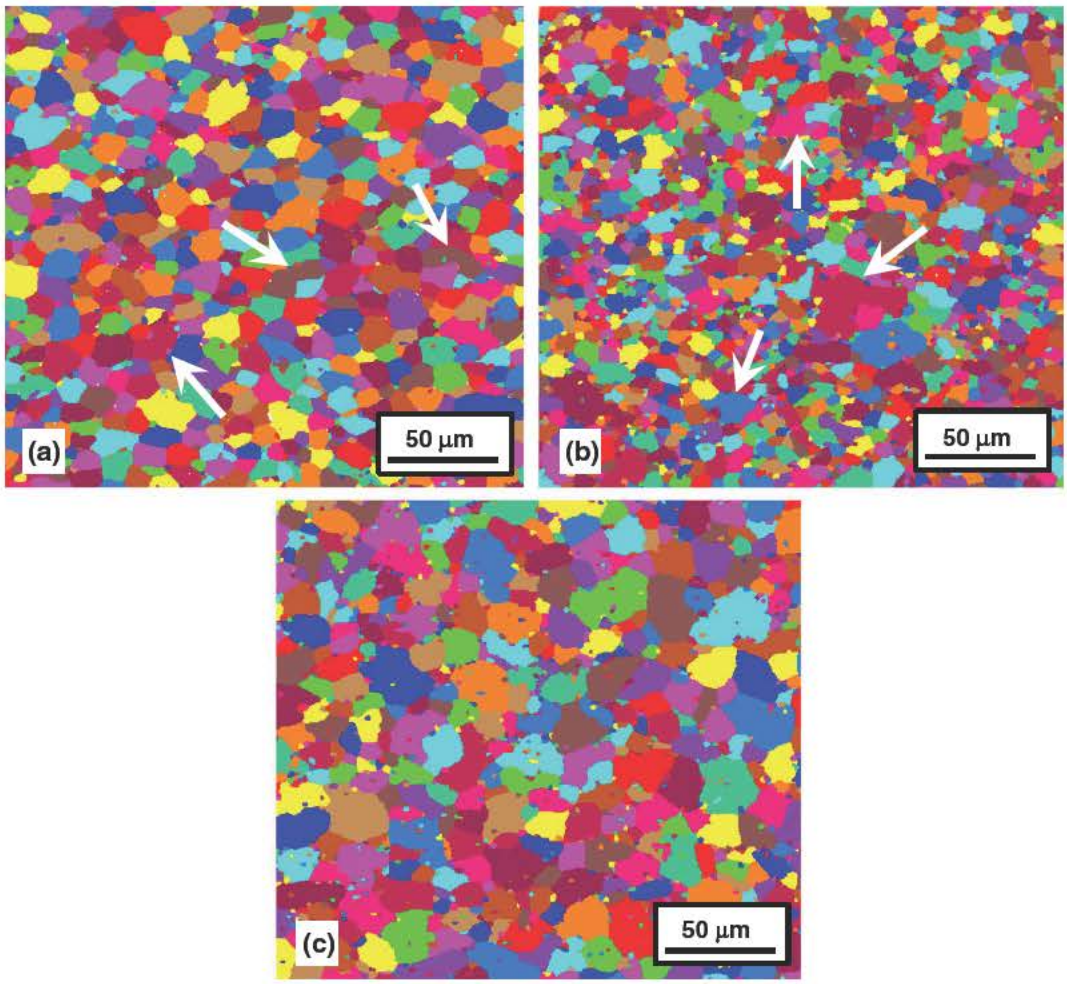

Fig. 8 EBSD grain ID maps for IN 100 samples compressed to a 2:1 height reduction at 1436 K (1163 °C) and a strain rate (s^{-1}) of (*a*) 0.001, (*b*) 0.01, or (*c*) 0.1.

Table VII. EBSD Grain-Size Data for LSHR Samples

Temp (K, °C)/ Strain Rate (s^{-1})	As Compressed Avg/ALA GS (μm)*	Compressed + SSHT Avg/ ALA GS (μm)**
(As Rec'd)		(13.6/48.0)
1339 (1066)/0.0005	2.1/7.3	15.5/67.9
1339 (1066)/0.01	1.7/6.4	12.8/48.9
1339 (1066)/1	1.1/15.4	13.6/48.6
1408 (1135)/0.0005	5.9/17.1	31.5/269.7
1408 (1135)/0.01	2.8/13.1	55.5/246.8
1408 (1135)/0.1	2.92/17.8	25.5/94.4
1408 (1135)/1	3.09/22.3	13.4/46.4
1408 (1135)/10	3.07/14.1	13.3/51.9

*Per segmented EBSD data, average as compressed gamma grain sizes for samples deformed at 1408 K (1135 °C) were 5.1 μm (0.01 s^{-1}), 5.1 μm (0.1 s^{-1}), 6.4 μm (1 s^{-1}), or 5.4 μm (10 s^{-1}).
**SSHT 1444 K (1171 °C)/1 h.

(Figures 11(b) through (d)) as well as for the shorter and longer exposure times (Figures 12(b), (d), (f) and 13). Even though there was some irregularity in the trends, by and large, these process parameters gave rise to an average grain size of ~80 to 110 μm and ALA:average grain size ratios of 3 to 5:1 (Tables V and VIII).

The grain structure developed during SSHT of IN-100 following pre-deformation at the highest strain rates (1, 10 s^{-1}), as well as a sample exposed 22 K (22 °C) below the solvus but not deformed, mirrored those developed in samples forged at lower temperatures. The grain structures were equiaxed (*e.g.*, Figure 11(f)), the average sizes were relatively small (~22 μm), and the ALA:average grain-size ratios (~3.5) (Table V) was comparable to that of the other normal-growth-like behaviors.

The grain structure developed during SSHT following pre-deformation at a strain rate of 0.1 s^{-1} had some aspects of the behaviors found for both the intermediate and highest strain rate regimes in terms of grain shapes (Figure 11(e)), average grain size (41.6 μm), and ALA:average grain-size ratio (3.3) (Table V).

Gamma-grain-size results for SSHT LSHR samples were similar to those for IN-100 (Table VII). For the as-received material and samples pre-deformed at a temperature of 1339 K (1066 °C), SSHT gave rise to a structure that was equiaxed and had a relatively fine grain size of ~15 μm in all cases. On the other hand, pre-deformation at 22 K (22 °C) below the solvus temperature [*i.e.*, at 1408 K (1135 °C)] gave rise to coarser gamma grain sizes. As for IN-100, the average size and ALA:average ratios for these latter LSHR samples

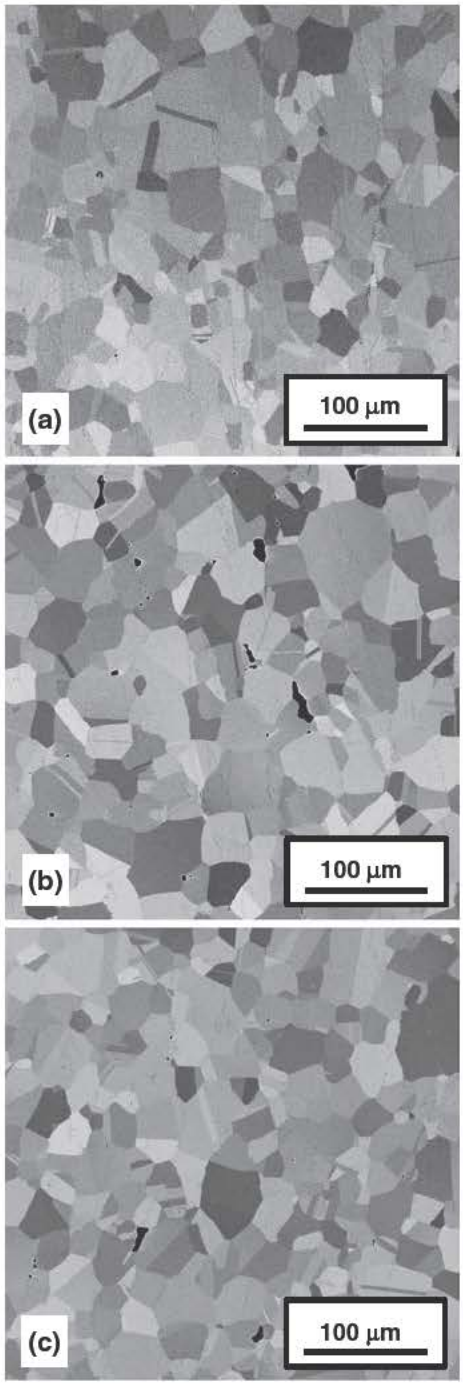

Fig. 9 BSE images illustrating the gamma grain structures devel oped in IN 100 during a 1 h SSHT of (*a*) an as received sample or samples pre deformed to a 2:1 height reduction at a strain rate of 0.001 s^{-1} and subsolvus temperature of (*b*) 1144 K (871 °C) or (*c*) 1255 K (982 °C).

could be separated into three regimes for pre-deformation strain rates which were low (0.0005 s^{-1}), intermediate (0.01 to 0.1 s^{-1}), and high (≥1 s^{-1}).

The inclusion of an additional subsolvus heat treatment prior to SSHT of LSHR samples pre-deformed at 1339 K (1066 °C) and a strain rate of 0.01, 0.1, or 10 s^{-1} had a minor effect on the final grain structure and size (Table IX).

IV. DISCUSSION

The key findings of this work can be interpreted in terms of the mechanisms of the hot deformation of the two PM superalloy program materials, IN-100 and LSHR, the associated driving forces for microstructure evolution during subsolvus hot working, and the effect of the subsolvus microstructure on subsequent supersolvus heat treatment (SSHT) response.

A. *Mechanisms of Hot Deformation*

The effect of strain rate and temperature on the mechanisms that controlled the deformation of the two program superalloys was similar to that observed in prior investigations[2 9] in which more restricted ranges of processing parameters were investigated. At relatively low temperatures (*i.e.*, T ~1144 K (871 °C), hot working over a wide range of strain rates (*e.g.*, 0.0003—10 s^{-1}) generally led to discontinuous dynamic recrystallization (DDRX). Similar behavior was found for hot working at intermediate temperatures [~1255 K (982 °C)], except for the lowest strain rate (0.0003 s^{-1}) at which superplastic flow was activated. DDRX generally resulted in similar refinement of the sizes of the gamma grains and the gamma-prime precipitates.

At 1339 K (1066 °C), a temperature comparable to that commonly used for isothermal forging of PM superalloys, there were also two discrete regimes of deformation: (1) low strain rates characterized by superplastic flow and near-constant grain size and (2) higher strain rates characterized by DDRX and gamma grain-size refinement. In all cases, coarse gamma-prime precipitates were preferentially located at the gamma grain boundaries for samples deformed at this temperature.

The broad aspects of plastic flow at 22 K (22 °C) below the gamma-prime solvus were similar to the findings for 1339 K (1066 °C) in that there appeared to be a transition in behavior as the strain rate was increased. However, there were some notable differences. First, marked flow hardening was observed at the lowest strain rates (<0.003 s^{-1}); this behavior was correlated to dynamic grain growth and led to the gradual loss of superplasticity with increasing strain. The grain growth was also accompanied by a tendency for the primary gamma-prime precipitates to separate from the gamma grain boundaries, such that approximately one-fourth of these particles lay within the gamma grains at the end of deformation. As the strain rate was increased, evidence of migration of the gamma grain boundaries, which was suggestive of DDRX, was noted. Such boundary migration and DDRX resulted however in gamma-grain-size *coarsening* and an increase with strain rate of the fraction of primary gamma precipitates lying away from the gamma grain boundaries.

B. *Subsolvus Hot Working: Driving Forces and Microstructure Evolution*

To interpret the observed variations of the as-deformed microstructures and their impact on SSHT

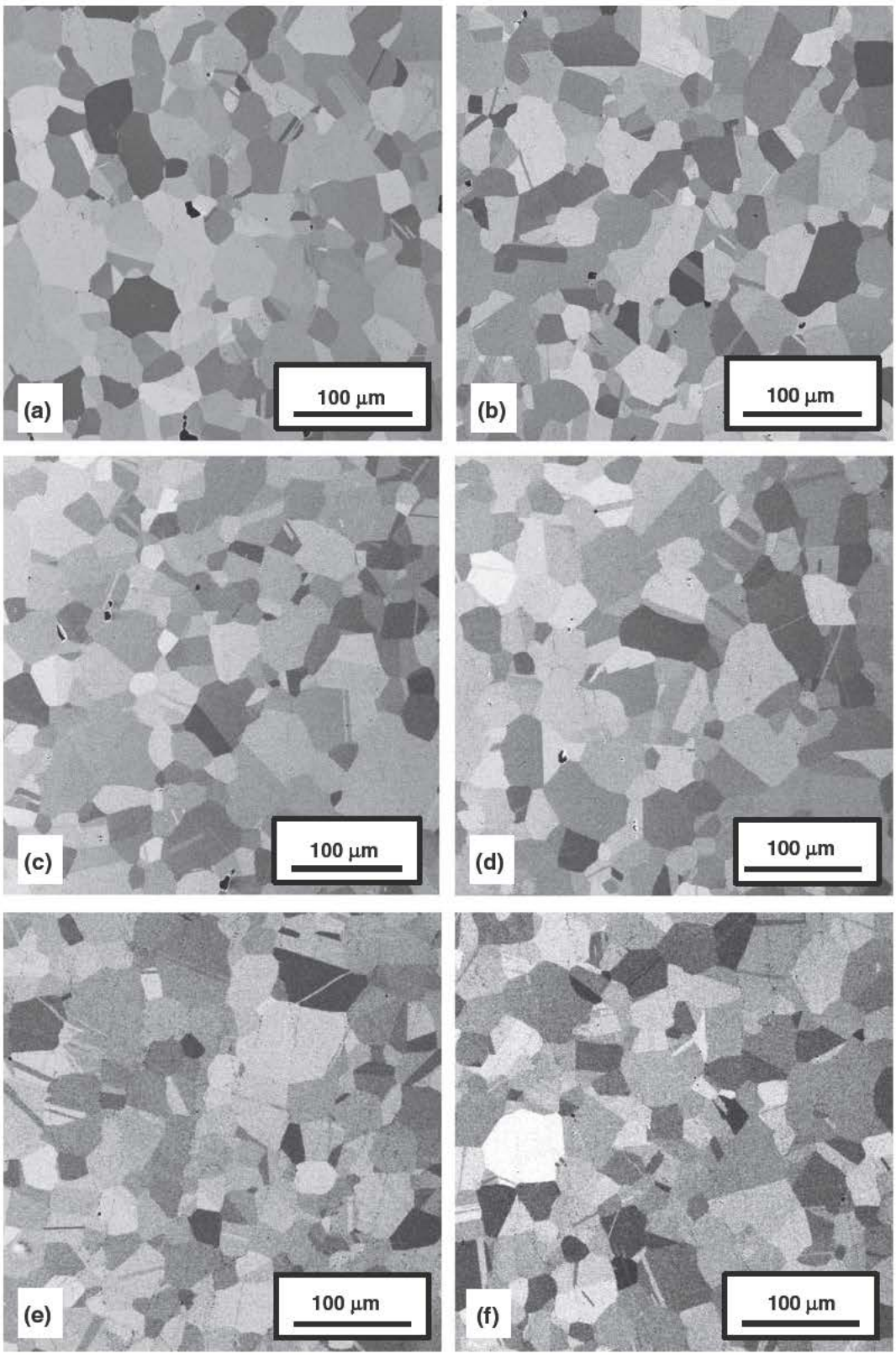

Fig. 10 BSE images illustrating the gamma grain structures developed in IN 100 during a 1 h SSHT of samples pre deformed to a 2:1 height reduction at 1339 K (1066 °C) and a strain rate (s^{-1}) of (*a*) 0.0003, (*b*) 0.001, (*c*) 0.003, (*d*) 0.01, (*e*) 0.1, or (*f*) 1.

response, the magnitude of the forces retarding or driving the migration of gamma grain boundaries at subtransus temperatures was estimated. The three principal forces were (1) the pinning pressure associated with gamma-prime precipitates, (2) the driving pressure associated with gamma grain growth and the reduction

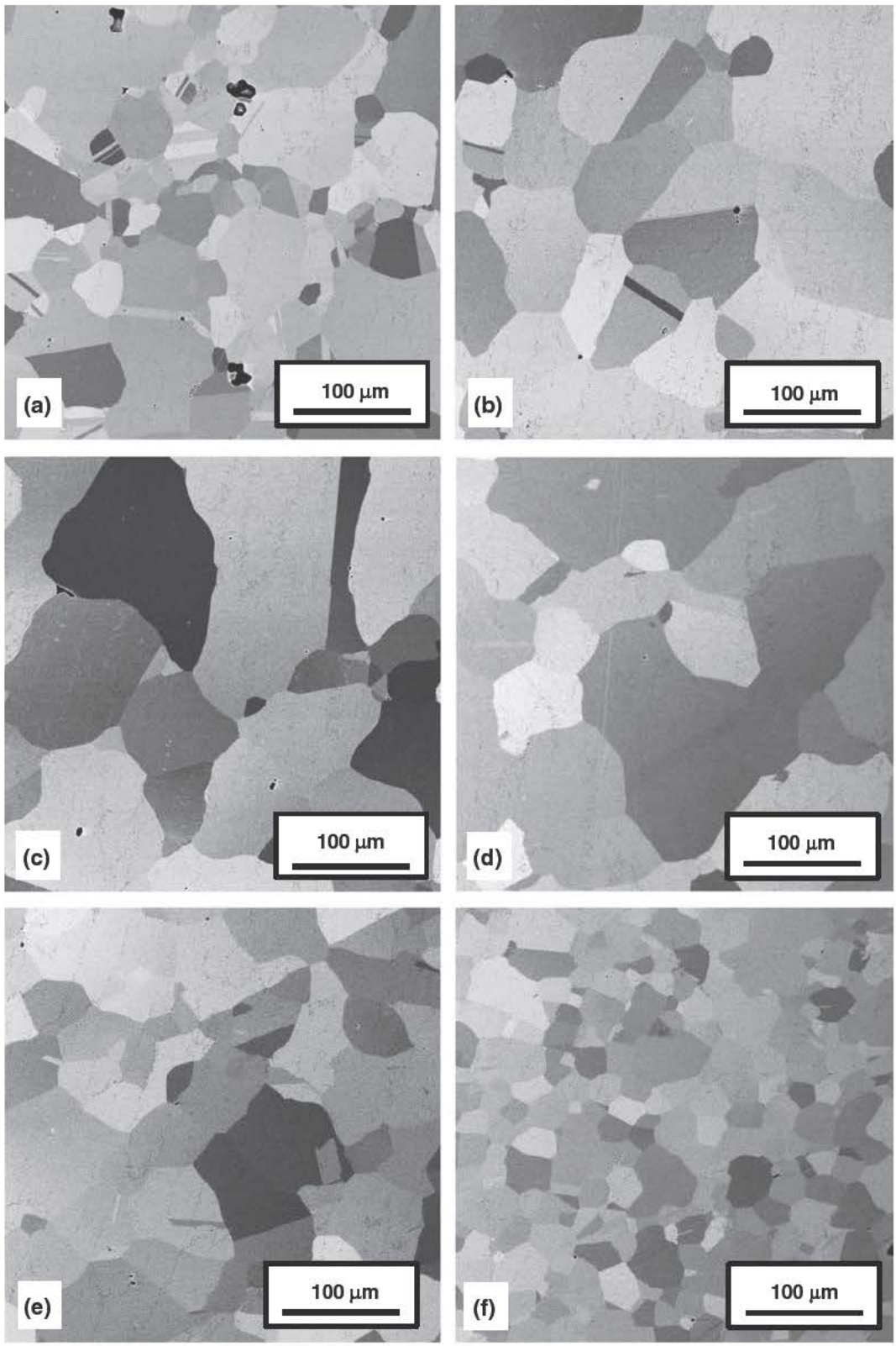

Fig. 11 BSE images illustrating the gamma grain structures developed in IN 100 during a 1 h SSHT of samples pre deformed to a 2:1 height reduction at 1436 K (1163 °C) and a strain rate (s^{-1}) of (*a*) 0.0003, (*b*) 0.001, (*c*) 0.003, (*d*) 0.01, (*e*) 0.1, or (*f*) 1.

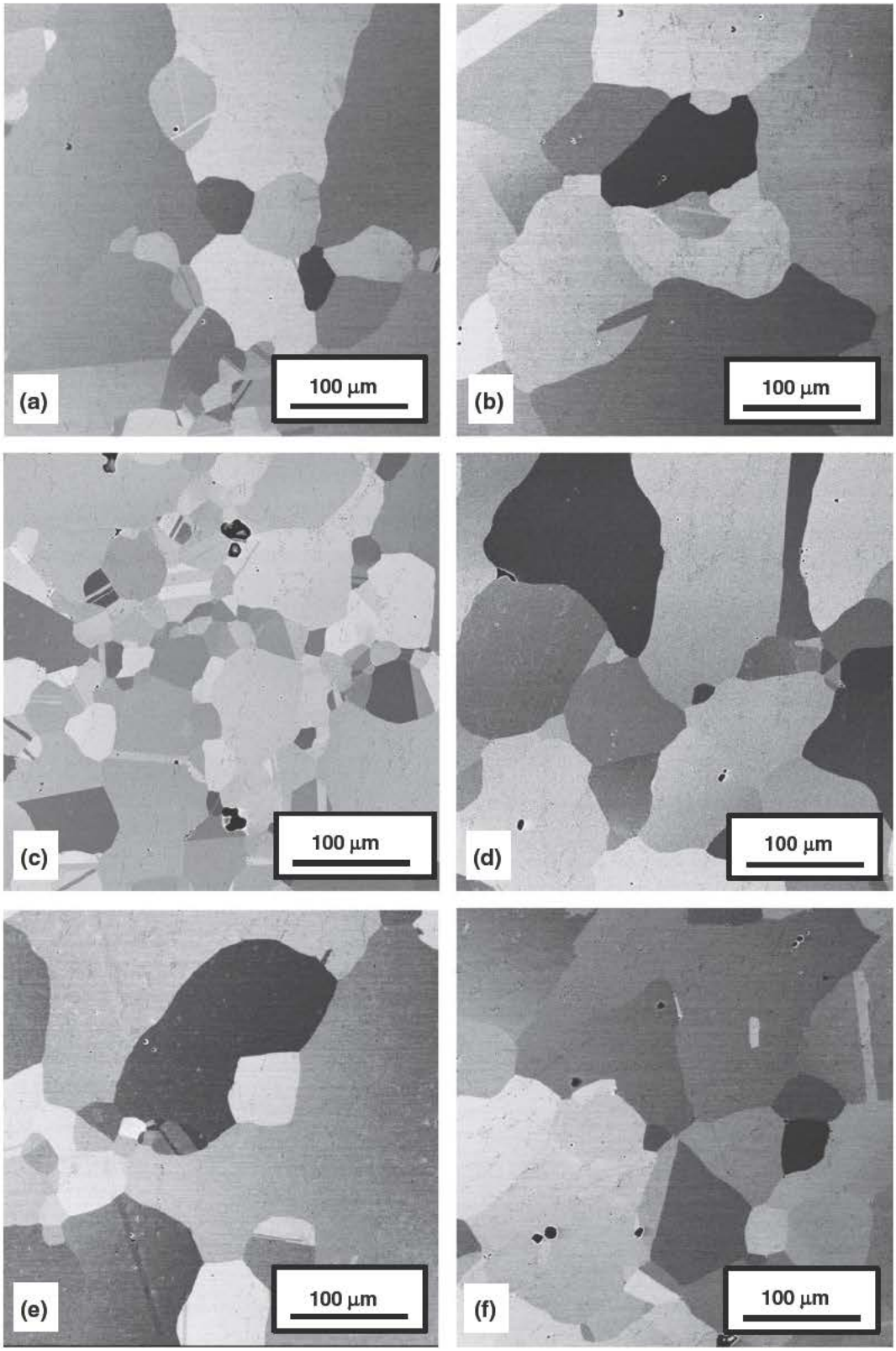

Fig. 12 BSE images illustrating the effect of SSHT time on the gamma grain structures developed in IN 100 pre deformed to a 2:1 height reduction at 1436 K (1163 °C) and a strain rate (s^{-1}) of (*a*, *c*, *e*) 0.0003 or (*b*, *d*, *f*) 0.003. The SSHT times (h) were (*a*, *b*) 0.25, (*c*, *d*) 1, or (*e*, *f*) 2.

Table VIII. Effect of Supersolvus Heat Treatment Time on EBSD Avg/ALA Grain Size (μm) in IN-100 Samples Pre-deformed at 1436 K (1163 °C)

Strain Rate (s^{-1})	0.05 h	0.25 h	1 h	2 h
0.0003		30.6/361.8	35.6/224.0	59.4/537.1
0.001	84.7/414.1		79.0/399.9	
0.003		108.9/493.2	90.3/309.6	101.9/489.3

Grain tolerance angle 5 deg, cleanup 10 pixels, SSHT temp 1477 K (1204 °C).

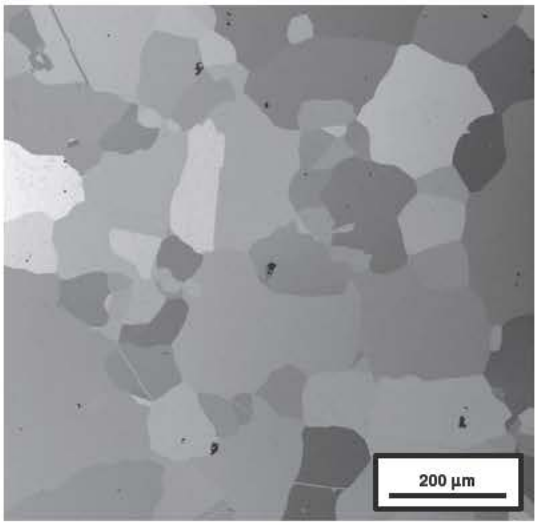

Fig. 13 BSE image illustrating the gamma grain microstructure developed during a 3 min SSHT in an IN 100 sample pre deformed to a 2:1 height reduction at 1436 K (1163 °C) and a strain rate 0.001 s^{-1}.

in grain-boundary surface energy, and (3) the driving pressure associated with the generation of dislocation substructure.

1. *Pinning pressure*

The pinning pressure, P_z, for a random distribution of precipitates whose volume fraction f_v is small is given by the classic Zener-Smith relation:[27,28]

$$P_z = 3f_v\Gamma_b/2r_p, \quad [1]$$

in which Γ_b and r_p denote the matrix-precipitate interface energy and gamma-prime precipitate radius, respectively.

When there is a large fraction (>0.01) of pinning particles, the particles tend to be highly correlated to the grain boundaries, and Eq. [1] no longer applies. In such cases, the particle spacing L is given by the approximate expression:[28]

$$L = (4\pi r_p^3/3f_v)^{1/3}. \quad [2]$$

At 1339 K (1066 °C), $r_p \sim 1$ μm and $f_v \sim 0.20$ for IN-100. Equation [2] thus yields $L \approx 2.8$ μm, or a value comparable to the *as-preheated* gamma grain size. In this case, a maximum pinning pressure, P_z^{max} is generated,[28] *i.e.*,

Table IX. EBSD Grain-Size Data for LSHR Samples Deformed at 1408 K (1135 °C) and Subjected to Various Heat Treatments

Strain Rate (s^{-1})	Heat Treatment [K (°C)]	Avg/ALA GS (μm)
0.01	1408 (1135)/1 h	4.6/19.3
0.01	1444 (1171)/1 h	55.5/246.8
0.01	1408 (1135)/1 h + 1444 (1171)/1 h	39.9/183.0
0.1	1408 (1135)/1 h	4.0/38.5
0.1	1444 (1171)/1 h	25.5/94.4
0.1	1408 (1135)/1 h + 1444 (1171)/1 h	21.0/66.0
10	1408 (1135)/1 h	4.4/17.8
10	1444 (1171)/1 h	13.3/51.9
10	1408 (1135)/1 h + 1444 (1171)/1 h	12.8/65.4

$$P_z^{max} = 1.2\Gamma_b f_v^{2/3}/r_p. \quad [3]$$

Taking $\Gamma_b = 1$ J/m^2 as representative of the interface energy for an incoherent gamma-prime precipitate in a gamma matrix, the pinning pressure was thus approximately 410,000 N/m^2.

At 1436 K (1163 °C), r_p~1 μm and f_v~0.05 for IN-100. Equation [2] yields $L \approx 4.4$ μm, a value somewhat less than the as-preheated gamma grain size, 6.7 μm. In this instance, the pinning pressure lies between the values calculated from Eq. [1] (75,000 N/m^2) and Eq. [3] (163,000 N/m^2).

2. *Driving pressure associated with grain-boundary energy*

The driving pressure P_g associated with gamma grain growth and the reduction in grain-boundary surface energy is $\alpha\Gamma_{gb}/R_\gamma$, in which α is a constant with a value in the range of 0.5 to 1, Γ_{gb} denotes the gamma grain-boundary energy, taken to be ~1 J/m^2 also, and R_γ is the average gamma-grain *radius*.[28] Taking $\alpha = 0.5$, this driving pressure was equal to approximately 500,000 N/m^2 when $R_\gamma \sim 1$ μm [for IN-100 at $T = 1339$ K (1066 °C)] or 153,000 N/m^2 when $R_\gamma = 3.25$ μm [for IN-100 at $T = 1436$ K (1163 °C)]. Thus, in the absence of deformation, the magnitudes of the pinning pressure and the driving pressure at each specific temperature were comparable, thereby providing a plausible explanation for the as-preheated grain sizes for IN-100 (Table V) as well as LSHR.

During near-superplastic deformation at 1436 K (1163 °C) and strain rates of 0.0003 and 0.001 s^{-1}, the gamma grains grew dynamically from ~6.7 to ~8.5 μm. In addition, flow hardening resulted in flow stress increases of the order of 50 percent during the imposed reduction. The increase in grain size (26 pct) was thus somewhat smaller than that which would be expected if both the grain-size and stress exponents of the strain rate were comparable, *i.e.*, ~2, as is common during superplastic flow. Although it was not easily measured, dynamic coarsening of gamma-prime precipitates was likely responsible for dynamic grain growth. Furthermore, the smaller gamma-prime particles that would have dissolved during the coarsening process would have allowed unpinning of some segments of the gamma grain boundaries, thus possibly producing some irregular grain shapes (prior to SSHT) due to grain-boundary migration.

3. *Driving pressure associated with deformation*

The balance between the particle-pinning and grain-growth driving pressures can be upset by deformation. Under low-strain-rate, superplastic conditions, imposed deformation is largely accommodated by boundary/interphase interface sliding; a relatively small amount of dislocation glide/climb within the matrix is activated to relieve stress concentrations generated at triple junctions.

When DDRX is activated under higher-strain-rate (and/or low temperature) conditions or as a result of dynamic grain growth, substantial dislocation densities and associated driving pressures are generated. In such cases, the flow stress σ and *average* dislocation density ρ are related as follows:[28]

$$\sigma = \alpha\mu b\sqrt{\rho}, \qquad [4]$$

in which α again is a constant between 0.5 and 1, μ is the shear modulus, and b is the length of the burgers vector. For grain boundary migration during DDRX, the maximum driving force is generated at the interface between a nascent nucleus (in which the dislocation density is zero) and the worked grain (with a dislocation density of ~ρ) into which it grows. The driving force P_d is then given by the following relation:[28]

$$P_d = \alpha\mu b^2\rho. \qquad [5]$$

For the PM superalloys of interest here, α is assumed to be 0.5, μ = 44 GPa at s ~ 1400 K (1127 °C),[29] and b ~2.5×10^{-10} m. For a flow stress of 50 MPa, the average dislocation density is thus obtained from Eq. [4] to be 1.14×10^{14} m^{-2}, and the driving pressure from Eq. [5] is 157,000 N/m^2. During DDRX at the high strains at which a steady-state flow stress is obtained, the dislocation density can vary from one grain to another depending on when the grain was most recently recrystallized. Hence, this estimate of the driving pressure must be considered as a *spatial* average.

The value of P_d can be interpreted in the context of the measured values of flow stress and microstructures developed in IN-100. At 1339 K (1066 °C), DDRX occurred at strain rates of ~0.01 s^{-1} and greater. The steady-state flow stress within this regime was 50 to 400 MPa, which would give rise to P_d between 157,000 and 1,256,000 N/m^2, or values approximately one-third to three times the pinning pressure associated with gamma-prime precipitates. Thus, the driving pressure associated with deformation would enhance the tendency for boundary migration a moderate amount or a great deal. However, the measured recrystallized grain sizes following deformation were *less* than the as-preheated size (Table V), suggesting that the rate of nucleation of new grains was very high and thus controlled the final grain size.

For deformation of IN-100 at 1436 K (1163 °C), gross DDRX started to occur at strain rates of 0.1 s^{-1} and greater at which flow stresses of the order of 75 to 150 MPa were developed, thus resulting in P_d of 236,000 to 471,000 N/m^2, or values much greater than the pinning pressure associated with the gamma-prime precipitates. Furthermore, deformation heating would have raised the sample temperature at the higher strain rates. Under adiabatic conditions, the temperature increase for a strain of 0.7 was estimated to be 9 K or 18 K (9 °C or 18 °C) for average flow stresses of 75 or 150 MPa. Because quantitative metallography revealed little change in the average size and volume fraction of the primary gamma-prime precipitates in the higher-rate samples, it may be concluded that deformation-induced temperature increases occurred over too short a time to lead to dissolution of the particles, however.

The strain-rate dependence of the microstructure developed in IN-100 (and LSHR) after deformation at a temperature 22 K (22 °C) below the solvus, and in particular the location of the gamma-prime precipitates relative to the gamma grain boundaries, can thus be rationalized on the basis of two competing effects, dynamic coarsening and DDRX. At low strain rates, dynamic coarsening would lead to a small increase in average gamma-prime precipitate size *via* the dissolution of the finer particles and growth of the coarser ones. This could lead to local unpinning of some gamma grain boundaries and their migration relative to the remaining precipitates as mentioned above. At high strain rates, the migration of all of the gamma grain boundaries would be enhanced due to DDRX and the associated moderate to high values of P_d relative to the pinning pressure. Thus, DDRX conditions would have tended to produce a microstructure in which most of the gamma grain boundaries had been able to break away from the precipitates and led to a recrystallized grain size which was greater than the as-preheated one. For intermediate strain rates, dynamic growth of some grains may have may have contributed to spatially non-uniform DDRX and the generation of dislocation-based driving pressures in the coarser grains, thus contributing to irregular grain shape and non-uniform distribution of gamma-prime precipitates relative to the gamma grain boundaries.

C. *Supersolvus Heat Treatment (SSHT) Response*

The SSHT response of IN-100 and LSHR can now be interpreted in terms of the microstructures developed

during prior-subsolvus deformation. In particular, the location of the gamma-prime precipitates relative to the gamma grain boundaries and sporadically-spaced, irregular grain shapes generated during the pre-deformation appeared to be the key factors which differentiated the evolution of the grain structure during subsequent SSHT.

For deformation temperatures of 1339 K (1066 °C) and below, the sizes of the gamma grains and gamma-prime precipitates were similar and, therefore, the precipitates were highly correlated to gamma grain boundaries. Thus, during the early stages of SSHT, the precipitates would be expected to dissolve (and relieve the pinning pressure associated with them) in a relatively uniform fashion. The gamma grains would then grow in a normal-like manner until they were pinned by the stable carbide and boride particles producing a microstructure of equiaxed grains (*e.g.*, Figures 9 and 10). Although both IN-100 and LSHR had comparable volume fractions and sizes of these stable minor phases, the pinned SSHT grain sizes differed by almost a factor of two, *i.e.*, ~25 μm for IN-100 and ~15 μm for LSHR. This difference may lie with the nature of the distribution of the carbide/boride particles; *i.e.*, they lay in stringers for IN-100, but were uniformly distributed for LSHR.

By contrast to the results for the lower temperatures, pre-deformation at 22 K (22 °C) below the solvus resulted in a noticeable strain-rate dependence of (1) the location of the gamma-prime precipitates relative to the gamma grain boundaries and (2) the uniformity of grain shape. Deformation at low-to-intermediate strain rates led to approximately 10 to 25 pct of the precipitates lying within the gamma grains and some non-equiaxed grains, while deformation at higher strain rates led to DDRX, an equiaxed grain structure, and the majority (≥70 pct) of the precipitates lying within the grains.

SSHT of samples pre-deformed near the solvus at low-to-intermediate strain rates led to large average grain sizes and grain structures that were noticeably irregular and non-equiaxed (Tables V and VII; Figures 11(a) through (e)). As suggested partially by previous experimental and theoretical work,[13,15,21] these observations may be attributable to the non-uniform dissolution of the gamma-prime precipitates and the irregular shape of a small fraction of the gamma grains (*e.g.*, with concave portions of grain boundary), possibly leading to subsequent non-uniform growth of the gamma grains during SSHT. For IN-100 pre-deformed 22 K (22 °C) below the solvus and a strain rate of 0.001 s^{-1}, the fact that essentially-identical coarse and non-equiaxed grain structures were developed after SSHTs for 3 minutes and 1 hours (Figures 11(b) and 13) suggests very rapid, abnormal-like behavior. Moreover, the short heat treatment time of 3 minutes above the solvus is comparable to that found experimentally for the dissolution of primary gamma-prime precipitates.[30] Furthermore, it may be hypothesized that the shapes of the irregular grains generated during subsolvus deformation, which appear to be a major factor in controlling the abnormal-like behavior, may be related to the distribution of gamma-prime precipitates. Future work could thus be beneficial in delineating the three-dimensional nature of such grains and gamma-prime precipitates and the influence of their irregular topology on abnormal-like behavior.

A related factor that may be pertinent to the SSHT response of samples forged near the solvus at low-to-intermediate strain rates is the nature of stored work. In this regard, plots of EBSD grain-reference-orientation-deviation (GROD) have been deduced to correlate qualitatively with dislocation substructure observed during transmission-electron microscopy of PM superalloys.[12] In prior work,[21] the levels and spatial distribution of GROD were found to be similar in

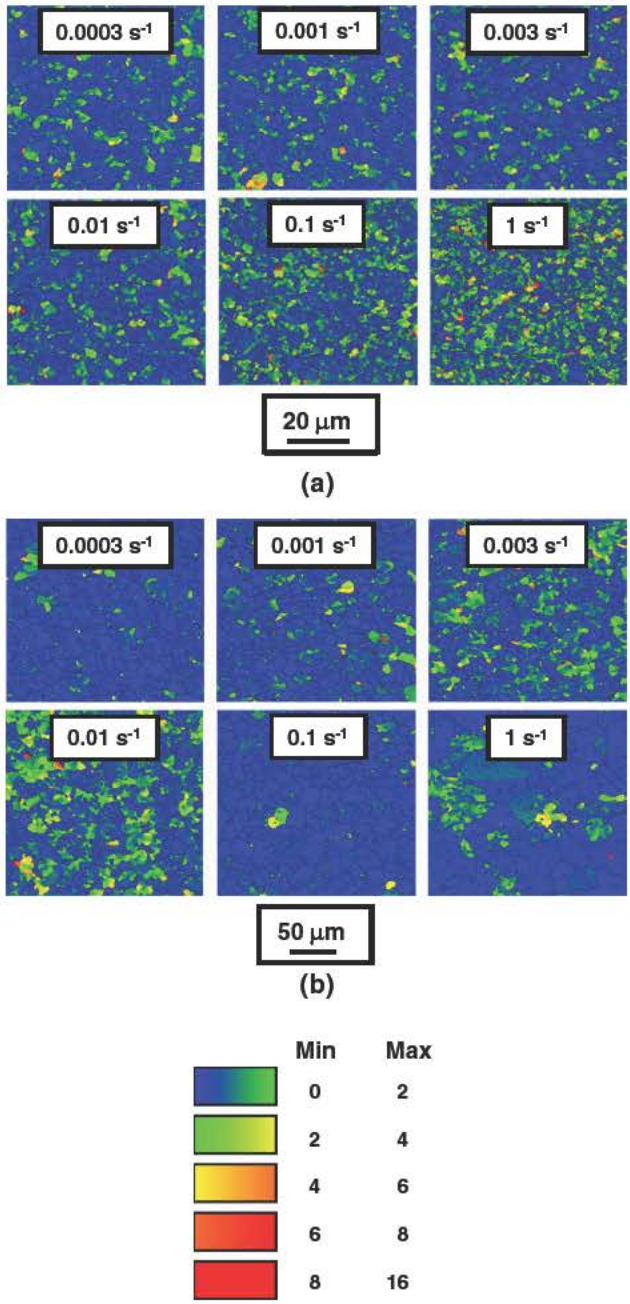

Fig. 14 EBSD grain reference orientation deviation (GROD) maps for IN 100 samples compressed at various strain rates and a temper ature (*a*) 1339 K (1066 °C) or (*b*) 1436 K (1163 °C).

Table X. EBSD GROD Data (in Pct) for As-Compressed IN-100 Samples

Temp [K (°C)]/Strain Rate (s^{-1})	0 to 2 deg	2 to 4 deg	4 to 6 deg	6 to 8 deg	8 to 16 deg
1339 (1066)/0.0003	93.1	5.9	0.8	0.1	0.0
1339 (1066)/0.001	93.1	5.5	1.1	0.1	0.1
1339 (1066)/0.003	93.6	5.4	0.8	0.1	0.1
1339 (1066)/0.01	90.6	7.1	1.7	0.5	0.1
1339 (1066)/0.1	85.6	10.5	2.7	0.8	0.4
1339 (1066)/1	79.4	14.3	4.1	1.4	0.8
1436 (1163)/0.0003	97.8	1.8	0.3	0.0	0.0
1436 (1163)/0.001	95.7	3.6	0.7	0.1	0.0
1436 (1163)/0.003	90.6	7.6	1.5	0.4	0.0
1436 (1163)/0.01	87.8	10.0	1.9	0.3	0.0
1436 (1163)/0.1	98.4	1.3	0.3	0.0	0.0
1436 (1163)/1	93.6	4.8	1.2	0.3	0.1

samples which did and did not exhibit abnormal-like grain-growth behavior during SSHT. GROD plots from the present work (Figure 14; Table X for IN-100) revealed similar, moderate levels (GROD ≤4 deg) and spatial uniformity of stored work for as-compressed samples deformed at a given strain rate and temperatures of 1339 K (1066 °C) or 1436 K (1163 °C) for which subsequent SSHT did not or did give rise to abnormal-like grain-growth behavior.

EBSD also revealed that the as-forged GROD values were largely unchanged during intermediate subsolvus heat treatment at the same temperature as the forging temperature. Payton[12] has shown that such residual stored work is eliminated only after heating above the gamma-prime solvus. The times required for this are *comparable to or less than* those required for the dissolution of gamma prime. Hence, the annihilation of dislocations and the dissolution of gamma-prime may interact in controlling the rate of release of the pinning force acting on the gamma grains, and certainly merits further investigation.

During SSHT, samples that had undergone DDRX during higher strain-rate, near-solvus pre-deformation developed relatively uniform, equiaxed-grain structures with an average size similar to those developed for lower-temperature pre-deformation (Tables V and VII; Figure 11(f)). Thus, it may be surmised that gamma-prime dissolution occurred relatively uniformly for these samples, and normal growth occurred until the gamma grains were pinned by the stable minor phases.

Last, prior theoretical work[15] has suggested that the development of abnormal-like grain structures such as those described herein is enhanced by the development of a small population of grains whose size exceeds the Zener-Smith limit prescribed by the minor phases which are stable above the solvus. The present results revealed that this may not be a necessary condition, however. For example, IN-100 samples deformed at 1436 K (1163 °C) and a strain rate of either 0.001 or 0.003 s^{-1} each developed a grain structure during deformation having ALA grains whose size (~24 μm) was almost identical to that developed during SSHT of samples pre-deformed at lower temperatures (Table V). The SSHT of these near-solvus-deformed samples gave rise to very coarse average grain sizes of the order of 90 to 100 μm. On the other hand, samples pre-deformed at this same temperature, but with a strain rate of 1 s^{-1}, gave rise to ALA grains which were much larger (~80 μm), but whose average grain size following SSHT was relatively fine (~22 μm).

V. SUMMARY AND CONCLUSIONS

Samples of two powder-metallurgy (PM) superalloys, IN-100 and LSHR, were isothermally compressed over a wide range of subsolvus temperatures and strain rates and then supersolvus heat treated (SSHT) to establish the effect of process variables on microstructure evolution. The principal findings of this work are summarized as follows:

1. Deformation at low hot working temperatures [200 K to 300 K, or (200 °C to 300 °C), below the gamma-prime solvus], or those below the temperature typically used to consolidate PM superalloy billet products, generally gives rise to discontinuous dynamic recrystallization (DDRX), thereby producing finer sizes of both the gamma grains and the gamma-prime precipitates. During subsequent SSHT, material thus pre-deformed develops an equiaxed structure with a gamma grain size of ~25 μm (IN-100) or ~15 μm (LSHR).
2. Subsolvus deformation at a temperature comparable to that at which isothermal forging of parts is typically conducted gives rise to superplastic flow and a nearly-constant size of the gamma grains and gamma-prime precipitates at low strain rates (~0.0003 to 0.01 s^{-1}). At higher strain rates (>0.01 s^{-1}), DDRX with concomitant microstructure refinement occurs. Despite the dependence of deformation mechanism on strain rate, subsequent SSHT gives rise to similar gamma grain sizes whose magnitude is essentially the same as that produced during SSHT of samples deformed in the low temperature range. Such a finding can be ascribed to the high degree of correlation of the gamma-prime precipitates with the gamma grain boundaries prior to and following deformation. Hence, the precipitates dissolve and the corresponding pinning pressure is released relatively uniformly during SSHT.

3. Deformation and microstructure evolution at a temperature 22 K (22 °C) below the gamma-prime solvus shows a strong dependence on strain rate. At low strain rates (of the order of 10^{-3} s^{-1}), superplastic flow at low strains is moderated by dynamic grain growth which results in reductions in the strain-rate sensitivity with increasing strain. Concurrently, a microstructure exhibiting a moderate fraction (~0.10 to 0.25) of gamma-prime precipitates lying within the gamma grains and some noticeably irregular grain shapes is developed. At intermediate strain rates (between approximately 3×10^{-3} and 0.1 s^{-1}), plastic flow characterized by a transition to DDRX behavior and similar as-deformed microstructural features is observed. During SSHT of samples pre-deformed within either the low- or intermediate-strain-rate regimes at 22 K (22 °C) below the solvus, microstructure development is characterized by gamma grains whose size is much larger than that produced using other subsolvus forging parameters. Such SSHT behavior appears to be abnormal-like in view of the very short times over which the microstructure is formed and the irregular shapes of the resulting gamma grains. It appears that this phenomenon may be related to the non-uniform dissolution of gamma-prime above the solvus and/or an irregular topology of the gamma grain structure produced during subsolvus deformation prior to SSHT.
4. Deformation at a temperature 22 K (22 °C) below the gamma-prime solvus and high strain rates (≥ 1 s^{-1}) is characterized by DDRX and a large dislocation-related driving force which enhances grain-boundary migration. Such a driving force results in an as-deformed microstructure of coarser gamma grains in which the majority of the gamma-prime precipitates lie *away from* the gamma grain boundaries. During SSHT of such material, uniform, equiaxed gamma grain structures with moderate grain sizes similar to those produced during the SSHT of samples pre-deformed at lower temperatures are developed. This behavior can also be ascribed to the uniformity of the dissolution of gamma-prime precipitates, which, in this case, lie primarily within the gamma grains prior to SSHT.

ACKNOWLEDGMENTS

This work was conducted as part of the in-house research of the Metals Branch of the Air Force Research Laboratory's Materials and Manufacturing Directorate. The support and encouragement of the Laboratory management are gratefully acknowledged. The authors thank P.N. Fagin and T.M. Brown for their yeoman service in conducting the experiments. Technical discussions with T.P. Gabb, A.D. Rollett, and E.J. Payton are also much appreciated. Three of the authors were supported under the auspices of contracts FA8650-08-D-5200 (JMS, ARS) and FA8650-09-2-5800 (WMS).

REFERENCES

1. M.J. Donachie Jr., ed.: *Superalloys Source Book*, ASM International, Materials Park, OH, 1984.
2. J. P.A. Immarigeon and P.H. Floyd: *Metall. Trans. A*, 1981, vol. 12A, pp. 1177 86.
3. A.K. Koul and J. P.A. Immarigeon: *Acta Metall.*, 1987, vol. 35, pp. 1791 05.
4. Y. Combres and C. Levaillant: *Int. J. Plast.*, 1990, vol. 6, pp. 505 19.
5. M.O. Alniak and F. Bedir: *Mater. Sci. Eng. A*, 2006, vol. A429, pp. 295 303.
6. M.O. Alniak and F. Bedir: *Mater. Sci. Eng. B*, 2006, vol. B130, pp. 254 63.
7. W. Tu and T.M. Pollock: in *Superalloys*, R.C. Reed, K.A. Green, P. Caron, T.P. Gabb, M.G. Fahrmann, E.S. Huron, and S.A. Woodard, eds., TMS, Warrendale, PA, 2008, pp. 395 403.
8. W.J. Tu: PhD Dissertation, University of Michigan, Ann Arbor, MI, 2010.
9. W.J. Tu and T.M. Pollock: *Metall. Mater. Trans. A*, 2010, vol. 41A, pp. 2002 09.
10. M. Soucail, M. Marty, and H. Ocor: in *Superalloys* 1996, R.D. Kissinger, D.J. Deye, D.L. Anton, A.D. Cetel, M.V. Nathal, T.M. Pollock, and D.A. Woodford, eds., TMS, Warrendale, PA, 1996, pp. 663 66.
11. E. Huron, S. Shrivatsa, and E. Raymond: in *Superalloys* 2000, T.M. Pollock, R.D. Kissinger, R.R. Bowman, K.A. Green, M. McLean, S. Olson, and J.J. Schirra, eds., TMS, Warrendale, PA, 2000, pp. 49 58.
12. E.J. Payton: PhD Dissertation, The Ohio State University, Columbus, OH, 2009.
13. P.R. Rios: *Acta Mater.*, 1997, vol. 45, pp. 1785 89.
14. K. Song and M. Aindow: *Proc. Mater. Sci. Technol. (MS&T) 2006: Fundamentals and Characterization*, vol. 2, Z K. Lu, C.E. Campbell, L.Q. Chen, E. B. Damm, J.E. Morral, and J.L. Murray, eds., TMS, Warrendale, PA, 2006, pp. 211 20.
15. G. Wang, D.S. Xu, E.J. Payton, N. Ma, R. Yang, M.J. Mills, and Y. Wang: *Acta Mater.*, 2011, vol. 59, pp. 4587 94.
16. T.P. Gabb, J. Gayda, and J. Falsey: Report NASA/TM 2005 213649, National Aeronautics and Space Administration, Glenn Research Center, Cleveland, OH, June 2005. http://gltrs.grc.nasa.gov.
17. D.D. Krueger, R.D. Kissinger, R.G. Menzies, and C.S. Wukusick: US Patent 4,957,567, September 1990.
18. E.L. Raymond, R.D. Kissinger, A.J. Paxson, and E.S. Huron: US Patent 5,584,947, December 1996.
19. E.S. Huron, J.A. Heaney, D.P. Mourer, J.R. Groh, E.L. Raymond, D A. Utah, M.J. Weimer, and K.R. Bain: US Patent Application 11/770,257, January 2009.
20. D.P. Mourer and K.R. Bain: US Patent Application 12/494,896, December 2010.
21. S.L. Semiatin, K. E. McClary, A.D. Rollett, C.G. Roberts, E.J. Payton, F. Zhang, and T.P. Gabb: *Metall. Mater. Trans. A*, 2013, vol. 44A, pp. 2778 98.
22. J. Gayda, T.P. Gabb, and P.T. Kantzos: in *Superalloys 2004*, K.A. Green, T.M. Pollock, H. Harada, T.E. Howson, R.C. Reed, J.J. Schirra, and S. Walston, eds., TMS, Warrendale, PA, 2004, pp. 323 30.
23. J. Lemsky: Report NASA/CR 2005 213574, Ladish Company, Inc., Cudahy, WI, February 2005. http://gltrs.grc.nasa.gov.
24. S.L. Semiatin, K.E. McClary, A.D. Rollett, C.G. Roberts, E.J. Payton, F. Zhang, and T.P. Gabb: *Metall. Mater. Trans. A*, 2012, vol. 43A, pp. 1649 61.
25. S.I. Wright: *Prakt. Metallogr.*, 2010, vol. 47, pp. 16 33.
26. A.A. Salem, M.G. Glavicic, and S.L. Semiatin: *Mater. Sci. Eng. A*, 2008, vol. A494, pp. 350 59.
27. C. Zener: Private Communication to C.S. Smith in *Trans. AIME*, 1948, vol. 175, pp. 15 51.
28. F.J. Humphreys and M. Hatherly: *Recrystallization and Related Phenomena*, Elsevier Science Ltd., Oxford, UK, 1996, chapters 3 and 9.
29. *Aerospace Structural Metals Handbook*, CINDAS LLC, West Lafayette, IN, 2000, vol. 5, code 4212.
30. E.J. Payton, T.A. Wynn, and M.J. Mills: *J. Mater. Sci.*, 2012, vol. 47, pp. 7305 11.